# PART III:
# Photochemistry and Vibrational Spectra of 1-Phenyl-tetrazolone Derivatives

## 3.3.1. Introduction

As focused earlier, most of the applications of tetrazolic compounds, in fields such as agriculture and medicine, are related with the acid/base properties of the tetrazolic ring. In fact, the tetrazolic acid fragment, $CN_4H$, has similar acidity to the carboxylic acid group, $CO_2H$, and is almost isosteric with it, but is metabolically more stable at physiologic pH.[1] The metabolic stability of the tetrazole ring strongly influences applications of its derivatives, including those containing the 5-oxy-substituent (tetrazolones). For instance, tetrazolone derivatives have been used as potent and selective agonists of the β3 human adrenergic receptors (β3-HAR).[2-5] The receptor is linked to the increase in metabolic rates in humans and, thus, β3-HAR agonists are useful in the treatment of obesity. Other β3-HAR agonists, containing imidazolidinone and imidazolone rings, were found to have quite low oral bioavailability due to their extensive metabolism. The higher stability of tetrazolone derivatives allowed to overcome this problem.[2-5] The use of tetrazole derivatives, including tetrazolones, in photography and photoimaging, has also been claimed by different patents.[6] In addition, tetrazolones have been used in inflating passenger restraint gas inflator bags.[7] From a more fundamental point-of-view, tetrazolones are also very interesting molecules, because they may exhibit different tautomers[8-15] and might be expected to have a very rich photochemistry.[16-19]

Hence, considering the important practical applications of tetrazolones and taking advantage of the unique capabilities of the matrix-isolation/FT-IR technique, an

investigation of the structure and photochemistry of two representative tetrazolones, 1-phenyl-tetrazolone (PT) and 1-phenyl-4-allyl-tetrazolone (PAT), was conducted, and is described herewith. Besides the structural and vibrational characterization of the matrix-isolated monomers of the compounds, their photochemical processes upon broad band UV-irradiation ($\lambda$ > 235 nm) were investigated. The interpretation of the experimental results was supported by extensive DFT calculations and, whenever available, also by previously reported reference matrix-isolation data on the putative photoproducts of PT and PAT.

As observed for 2-methyl-2*H*-tetrazol-5-amine (2MTA), 1-phenyl-tetrazolone (PT) can exist in different tautomeric forms. In this particular case, they are associated with keto-enol tautomeric equilibria. On the other hand, 1-phenyl-4-allyl-tetrazolone (PAT) is a molecule without labile hydrogen atoms (thus simplifying the system in terms of tautomerism) but with a conformationally flexible substituent (allyl group; $-CH_2-CH=CH_2$). Our interest in the investigation of 4-allyl-tetrazolones was also motivated by the fact that these compounds are important synthetically, as precursors of other biologically active heterocycles.[20]

Thus, the molecular structure, vibrational spectra and photochemistry of the derivatives of tetrazole, 1-phenyl-tetrazolone (PT) and 1-phenyl-4-allyl-tetrazolone (PAT), have been studied by FT-IR matrix isolation spectroscopy and DFT/B3LYP/611++G(d,p) calculations.

Among the five structures in which PT could be expected to exist (two keto tautomers, one mesoionic olate-form and two different conformers of the hydroxyl tautomer), only the most stable species, 1-phenyl-1,4-dihydro-5*H*-tetrazol-5-one, could be experimentally observed in low temperature argon matrices. Monomers of this tautomer give rise to an IR spectrum that fits nicely the calculated spectrum obtained at

the DFT/B3LYP/6-311++G(d,p) level of theory. *In situ* UV-irradiation ($\lambda$ > 235 nm) of the matrix-isolated PT induces three main photochemical processes, all of them involving cleavage of the tetrazole ring: *(1)* molecular nitrogen loss, with production of 1-phenyl-diaziridin-3-one; this compound reacts subsequently to form 1-aza-1,2,4,6-cycloheptatetraene and isocyanic acid (eventually, also to form CO plus phenyldiazene); *(2)* cleavage of the $C_{(5)}$–$N_{(1)}$ and $N_{(3)}$–$N_{(4)}$ tetrazole-ring bonds, with production of phenylazide and isocyanic acid, with phenylazide then losing $N_2$ to yield as final product 1-aza-1,2,4,6-cycloheptatetraene; and *(3)* cleavage of the $N_{(1)}$–$N_{(2)}$ and $N_{(4)}$–$C_{(5)}$ tetrazole-ring bonds, to yield phenylisocyanate and azide.

*In situ* UV-irradiation ($\lambda$ > 235 nm) of matrix-isolated PAT also induces three types of photofragmentation: *(1)* production of phenylazide and allylisocyanate, with phenylazide then losing $N_2$ to yield 1-aza-1,2,4,6-cycloheptatetraene; *(2)* formation of phenylisocyanate and allylazide; and *(3)* $N_2$ elimination leading to formation of 1-allyl-2-phenyldiaziridin-3-one; this compound partially reacts further to form 1-allyl-1*H*-benzoimidazol-2(3*H*)-one. The observed photochemistry of the matrix-isolated PAT is distinct from the preferred photochemical fragmentation in solution, where 3,4-dihydro-3-phenylpyrimidin-2(1*H*)-one is produced as the sole primary photoproduct.

## 3.3.2. Photochemistry of 1-Phenyl-tetrazolone Isolated in Solid Argon

- DFT structural calculations: tautomerism and molecular geometry

According to the DFT/B3LYP/6-311++G(d,p) calculations, PT can exist in five tautomeric forms: two keto tautomers, one mesoionic olate form and two hydroxy conformers (Figure 1). Two of these species (the most stable keto form and the olate

tautomer) are planar structures, belonging to the $C_S$ symmetry point group, whereas the remaining three forms are non-planar structures ($C_1$ point group).

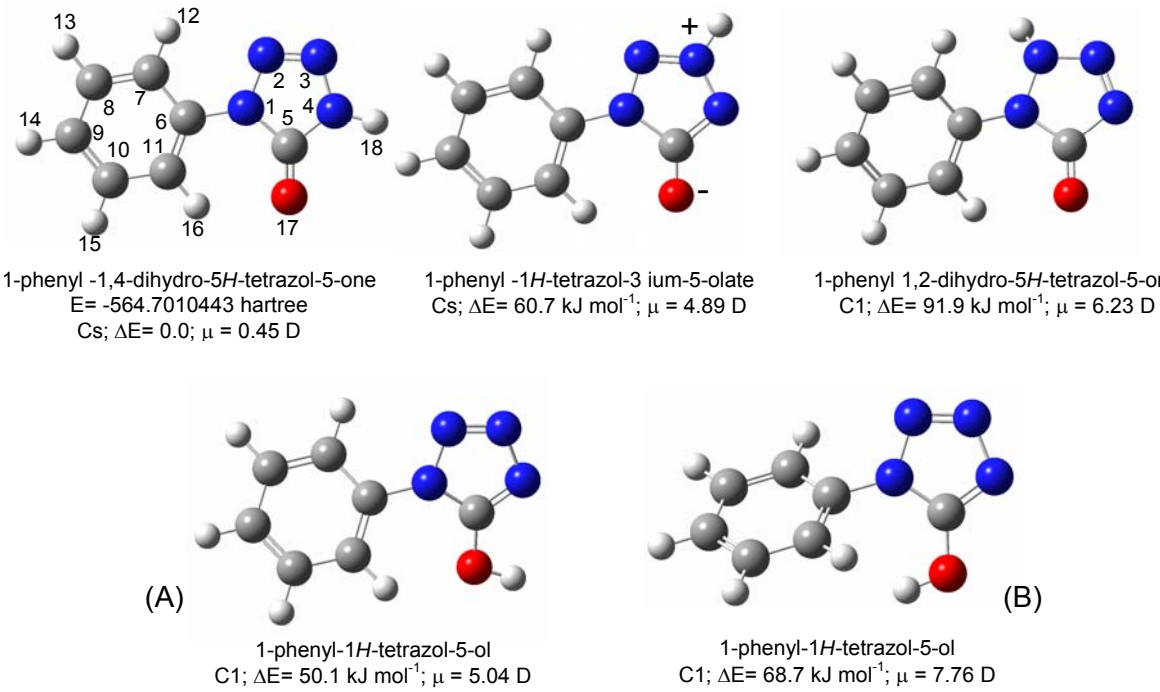


1-phenyl -1,4-dihydro-5*H*-tetrazol-5-one
E= -564.7010443 hartree
Cs; ΔE= 0.0; μ = 0.45 D

1-phenyl -1*H*-tetrazol-3 ium-5-olate
Cs; ΔE= 60.7 kJ mol$^{-1}$; μ = 4.89 D

1-phenyl 1,2-dihydro-5*H*-tetrazol-5-one
C1; ΔE= 91.9 kJ mol$^{-1}$; μ = 6.23 D

1-phenyl-1*H*-tetrazol-5-ol
C1; ΔE= 50.1 kJ mol$^{-1}$; μ = 5.04 D

1-phenyl-1*H*-tetrazol-5-ol
C1; ΔE= 68.7 kJ mol$^{-1}$; μ = 7.76 D

**Figure 1.** Tautomers of 1-phenyltetrazolone (PT) with atom numbering. Symmetry point groups and dipole moments and relative energies (including zero point vibrational energies) calculated at the B3LYP/6-311++G(d,p) level of theory are also given.

The 1-phenyl-tetrazolone keto tautomer 1-phenyl-1,4-dihydro-5*H*-tetrazol-5-one was predicted to be considerably more stable than all the remaining species. Part of the stabilization of this form results from the favorable interactions between the phenyl hydrogen atoms *ortho* to the tetrazole ring, $H_{(12)}$ and $H_{(16)}$, and the $N_{(2)}$ and carbonyl oxygen atoms, respectively (see Figure 1). These interactions also partially justify the fact that the two rings (phenyl and tetrazole) stay in the same plane. The second most stable form is one of the two hydroxy forms (conformer A of 1-phenyl-1*H*-tetrazol-5-ol; Figure 1) and has an energy higher than the most stable species by *ca.* 50 kJ mol$^{-1}$. In this hydroxy conformer, the hydroxylic hydrogen atom points to the opposite direction relatively to the phenyl group, whereas in the higher energy hydroxy conformer (form B, with relative energy of *ca.* 70 kJ mol$^{-1}$) this hydrogen atom and the phenyl group

point nearly to each other. In conformer A, the optimization of the interaction between $H_{(16)}$ and the hydroxylic oxygen atom (which contrarily to the carbonyl oxygen in the most stable keto tautomer has its lone-electron pairs out of the plane of the tetrazole ring) is responsible for the deviation of the molecule from planarity. According to the calculations, the $C_{(11)}$–$C_{(6)}$–$N_{(1)}$–$C_{(5)}$ inter-ring dihedral angle in this molecule is 30.3°. On the other hand, in conformer B, a strong steric interaction between $H_{(16)}$ and the hydroxylic hydrogen atom takes place and leads to a much larger deviation of the molecule from planarity, the $C_{(11)}$–$C_{(6)}$–$N_{(1)}$–$C_{(5)}$ inter-ring dihedral angle being predicted by the calculations as 52.2°. The second keto tautomer and the olate form differ from the most stable tautomer essentially in the position of the tetrazole ring hydrogen atom. The olate tautomer is predicted by the calculations as the third most stable form, with a relative energy of *ca.* 60 kJ $mol^{-1}$. Like the most stable tautomer, the olate form has a planar structure, since in this case the stabilization of the planar geometry resulting from favorable interactions between the phenyl hydrogen atoms *ortho* to the tetrazole ring, $H_{(12)}$ and $H_{(16)}$, and the $N_{(2)}$ and oxygen atoms, do also take place. On the other hand, the second keto tautomer, 1-phenyl-1,2-dihydro-5*H*-tetrazol-5-one (Figure 1), is non-planar, with an inter-ring dihedral angle of 34.2° and the nitrogen atom bearing the hydrogen atom considerably pyramidalized (the calculated $N_{(1)}$–$N_{(2)}$–($H_{(18)}$)–$N_{(3)}$ dihedral angle is 129.9°), due to the proximity between the hydrogen atom bonded to the tetrazole ring and $H_{(12)}$. This form corresponds to the highest energy tautomer, with a relative energy of *ca.* 92 kJ $mol^{-1}$. The fully optimized geometries for all TP tautomers are provided in Table S1 (Appendix D).

- Infrared spectrum of the matrix-isolated compound (as-deposited matrix)

Considering the relative energies of the five tautomers of PT, only the most stable form is expectable to be present in the gaseous phase and trapped in the low temperature matrices. Indeed, the IR spectrum of the as-deposited PT Ar-matrix nicely fits the calculated spectrum of 1-phenyl-1,4-dihydro-5*H*-tetrazol-5-one (Figure 2). Table 1 displays the proposed band assignments. Table S2 (Appendix D) shows the definition of the internal coordinates used to perform the normal coordinate analysis made in this study, which is presented in Table S3 (Appendix D).

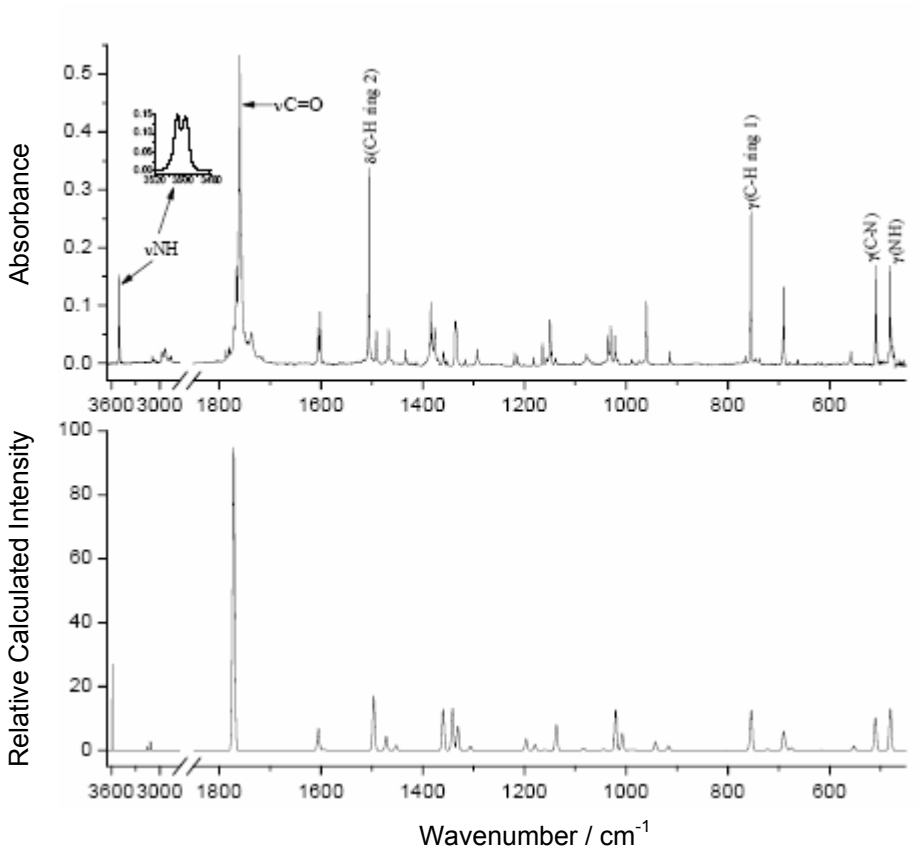


**Figure 2.** Infrared spectra of PT: upper panel, isolated in an argon matrix (as-deposited matrix; substrate temperature, 10 K; nozzle temperature, 369K; bands due to traces of monomeric water subtracted). Lower panel, DFT/B3LYP/6-311++G(d,p) calculated spectrum for the minimum energy conformation. Calculated spectra were simulated using Gaussian functions centered at the calculated (scaled by 0.978) frequency and with bandwidth at half height equal to 5 $cm^{-1}$.

It can be observed in Figure 2 that most of the bands in the experimental spectrum appear split due to the existence of different matrix sites. Extensive site splitting has also been observed previously for other tetrazoles isolated in argon matrices.[8,9,21,22] The most intense bands of the PT spectrum are due to the νN–H, νC=O, δ(C–H ring 2), γ(C–H ring 1), γC–N and γN–H modes. The νN–H vibration gives rise to a triplet of bands, at 3503.9, 3498.2 and 3496.9 $cm^{-1}$, indicating that the local environment around the NH group in the various possible matrix sites occupied by the PT molecule in the argon matrix can be essentially of three different types. This fact is reinforced by the observation that the δNH mode does also give rise to a triplet of bands near 1335 $cm^{-1}$. On the other hand, the γNH mode gives rise to only one main band, at 481.0 $cm^{-1}$, pointing to a similar intermolecular potential for out-of-plane deformation of the tetrazole-ring hydrogen atom in all three main matrix sites. These results can also be correlated with the planarity of the guest molecule, which can fit into a single layer of closely packed argon atoms (implying similar stacking interactions), but with mismatching longitudinal environments. The most intense band corresponds to the νC=O vibrational mode and appears as a group of, at least, nine bands. It corresponds to approximately the third part of the whole area under the spectrum (31%), in good consonance with the theoretical predictions (34%).

The δ(C–H ring 2) vibrational mode corresponds to the symmetric (relatively to a plane perpendicular to the phenyl-ring passing through $C_{(6)}$ and $C_{(9)}$) bending mode of the four phenyl hydrogen atoms placed at the *ortho* and *meta* positions relatively to the tetrazole fragment. The calculated intensity for this vibrational mode is similar in PT (90.7 km $mol^{-1}$) and in 1-phenyltetrazole (82.1 km $mol^{-1}$)[23], but nearly twice those found in 5-chloro-1-phenyltetrazole (57.5 km $mol^{-1}$)[23] and chlorobenzene (45.5 km $mol^{-1}$), being much more intense than in other monosubstituted phenyl compounds,

such as for example benzyl or 1-phenyl-1,2-propanedione[24,25] [in benzyl the δ(C–H ring 2) *asym* and δ(C–H ring 2) *sym* modes, are predicted to give rise to bands with intensity equal to 0.9 and 0.7 km $mol^{-1}$, respectively;[24] in 1-phenyl-1,2-propanedione, the predicted intensity for this mode is 0.6 km $mol^{-1}$][25]. These results indicate that this vibration is very sensitive to substituent effects. On the other hand, it does not appear to be very sensitive to matrix local environment, since for the above compounds existing in more than one site in argon matrices it has been systematically observed as a single band.[23-25] Very interestingly, this is just the opposite situation compared to γ(C–H ring 1), whose calculated intensity in PT (66.7 km $mol^{-1}$) does not differ very much from those found in other phenyl monosubstituted molecules (*e.g.*, 1-phenyltetrazole, 44.1 km $mol^{-1}$; 5-chloro-1-phenyltetrazole, 35.1 km $mol^{-1}$, chlorobenzene, 62.7 km $mol^{-1}$; benzyl, 38.6 and 50.2 km $mol^{-1}$, for the antisymmetric and symmetric mode, respectively;[24] terphenyl, 75.2 km $mol^{-1}$),[26] but are usually observed as a site-split multiplet (*i.e.*, this mode seems to be relatively little affected by substitution, but it is quite sensitive to the matrix local environment).

The remaining intense band in the spectrum of PT is due to the γCN coordinate, which corresponds to the out of plane vibration leading to pyramidalization of $N_{(1)}$. This band is observed around 500 $cm^{-1}$, at a position similar to those found for the equivalent vibrations in other 1-phenyl-substituted tetrazoles.[23] In both 1-phenyltetrazole and 5-chloro-1-phenyltetrazole[23] the γCN band was found to be less intense than in PT (calculated intensities are *ca.* 10 in these two compounds, versus 55 km $mol^{-1}$ in PT). This result is consistent with a higher degree of polarization of the $C_{(5)}$–$N_{(1)}$ bond in PT due to the presence of the oxygen substituent linked to $C_{(5)}$, and can also be correlated with the considerably longer $C_{(5)}$–$N_{(1)}$ bond length (140.0 pm) and smaller $\nu C_{(5)}$–$N_{(1)}$ stretching frequency (*ca.* 960 $cm^{-1}$) found in this molecule, when compared with the

corresponding values in both 1-phenyltetrazole and 5-chloro-1-phenyltetrazole (135.3 pm and *ca.* 1205 $cm^{-1}$ and 135.7 pm and *ca.* 1240 $cm^{-1}$, respectively[23]).

**Table 1.** Observed frequencies ($cm^{-1}$) for PT in argon matrices.[a]

| Approximate Description | Calculated frequency | Intensity | Observed Frequency Ar (9 K) | I |
|---|---|---|---|---|
| νN–H | 3585.7 | 144.1 | 3503.9/3498.2/3496.9 | S/S/sh |
| ν(C–H ring 2) | 3159.7 | 6.7 | 3475.8 | w |
| ν(C–H ring 1) | 3149.3 | 0.3 | 3072.8/3059.0/3049.4 | w/w/w |
| ν(C–H ring 3) | 3122.3 | 15.1 | 2970.6/2935.3 | w/w |
| ν(C–Hring 4) | 3110.4 | 13.3 | 2883.7/2862.9 | w/w |
| ν(C–H ring 5) | 3100.2 | <0.1 | n.o. | |
| νC=O | 1771.7 | 507.8 | 1786.8/ 1780.7/1770.7/ 1765.9/1759.7/1757.1/ 1749.7/1744.0/1736.1 | w/w/w/ w/S/sh/ m/w/w |
| ν(C–C ring 2) | 1604.8 | 36.6 | 1605.6/1601.6 | m/m |
| ν(C–C ring 4) | 1593.9 | 1.6 | 1595.9/1593.3 | m/w |
| δ(C–H ring 2) | 1496.3 | 90.7 | 1505.2 | S |
| νN=N | 1471.8 | 23.5 | 1490.8 | m |
| ν(C–C ring 3) | 1452.3 | 8.2 | 1467.4 | m |
| νN–C (inter ring) | 1359.7 | 68.6 | 1386.6/1384.0/ 1376.4/1369.9/1359.4 | w/m m/w/w/ |
| δNH | 1341.3 | 70.8 | 1336.5/1334.8/ 1333.3 | m/m/ sh |
| δ(C–H ring 1) | 1330.8 | 40.1 | 1320.1/1316.6 | w/w |
| ν(C–C ring 3) | 1306.1 | 6.9 | 1293.2 | m |
| νN–C | 1196.9 | 19.0 | 1219.4/1213.0/1200.8 | w/w/w |
| δ(C–H ring 4) | 1179.2 | 9.7 | 1188.6/1181.8 | w/w |
| δ(C–H ring 5) | 1159.5 | 0.8 | 1171.0 | w |
| νN–N (1,2) | 1137.3 | 42.7 | 1164.6/1156.2/1149.8/ /1146.1/1138.9 | m/w/m w/w |
| δ(C–H ring 6) | 1083.5 | 3.5 | 1103.0/1078.2 | w/w |
| ν(C–C ring 5) | 1044.3 | 1.3 | 1044.9 | w |
| νN–N (3,4) | 1020.7 | 68.1 | 1035.8//1030.3 | m/m |
| δ(ring 1) | 1007.7 | 28.6 | 1022.4/1019.9/1010.3 | m/m/w |
| ν(C–C ring 1) | 992.6 | 0.4 | 1000.3 | w |
| γ(C–H ring 5) | 984.7 | 0.6 | 989.0/984.1 | w/w |
| τ(ring 3) | 971.5 | <0.1 | 974.6/972.4 | w/w |
| νN–C | 942.2 | 14.2 | 964.8/960.6 | w/m |
| γ(C–H ring 3) | 916.6 | 7.4 | 914.2 | m |
| γ(C–H ring 2) | 838.2 | <0.1 | n.o. | |
| δ(Nring 1) | 758.5 | 2.2 | 765.3 | w |
| γ(C–H ring 1) | 754.0 | 66.7 | 754.6/747.9/746.2 | S/w/w |
| γC=O | 721.7 | 1.4 | 736.8 | w |
| τ(ring 1) | 690.6 | 30.4 | 690.5 | m |
| δ(ring 3) | 686.6 | 9.1 | 679.0 | w |
| τ(Nring 1) | 675.1 | 4.7 | 663.5/661.9 | w/w |
| δ(ring 2) | 617.0 | 0.2 | 616.2 | w |
| δC=O | 552.3 | 7.0 | 558.0 | w |
| γCN | 510.0 | 54.1 | 509.4 | m |
| γN–H | 480.7 | 69.3 | 484.1/481.0/478.9 476.2/473.6 | w/m/w w/w |
| γ(C–H ring 4) | 408.4 | <0.1 | n.i. | n.i. |
| δCN | 371.4 | 0.6 | n.i. | n.i. |
| δ(Nring 2) | 318.6 | 6.3 | n.i. | n.i. |
| τ(ring 2) | 286.5 | 0.8 | n.i. | n.i. |
| τ(Nring 2) | 218.1 | 1.8 | n.i. | n.i. |
| δNC | 173.7 | 1.5 | n.i. | n.i. |
| γNC | 97.7 | 2.9 | n.i. | n.i. |
| τ(C–N) | 24.0 | <0.1 | n.i. | n.i. |

DFT(B3LYP)/6-311++G(d,p) calculated frequencies and intensities (km $mol^{-1}$) are given for comparison. See Table S2 (Appendix D) for definition of internal coordinates.[a] I, intensity; ν, bond stretching; δ, bending; γ, rocking; τ, torsion; S, strong; m, medium; w, weak; sh, shoulder; n.o., not observed; n.i., not investigated.

- *In situ* UV-irradiation experiments ($\lambda > 235$ nm)

*In situ* UV-irradiation ($\lambda > 235$ nm) of the matrix isolated PT monomers led to fast consumption of this compound (≈50% in 5 min) and appearance of bands due to photochemical products. The results are summarized in Figures 3 and 4 and Table 2. Figure 3 shows, in a schematic way, the reaction paths leading to the different observed photoproducts. These were proposed taking into consideration the analysis of the spectroscopic results, supported by calculations and previously available experimental data on putative photoproducts. The suggested band assignments are summarized in Table 2. A complete list of calculated frequencies and intensities for the observed photoproducts and other relevant chemical species is provided in Tables S4–S17 (Appendix D).

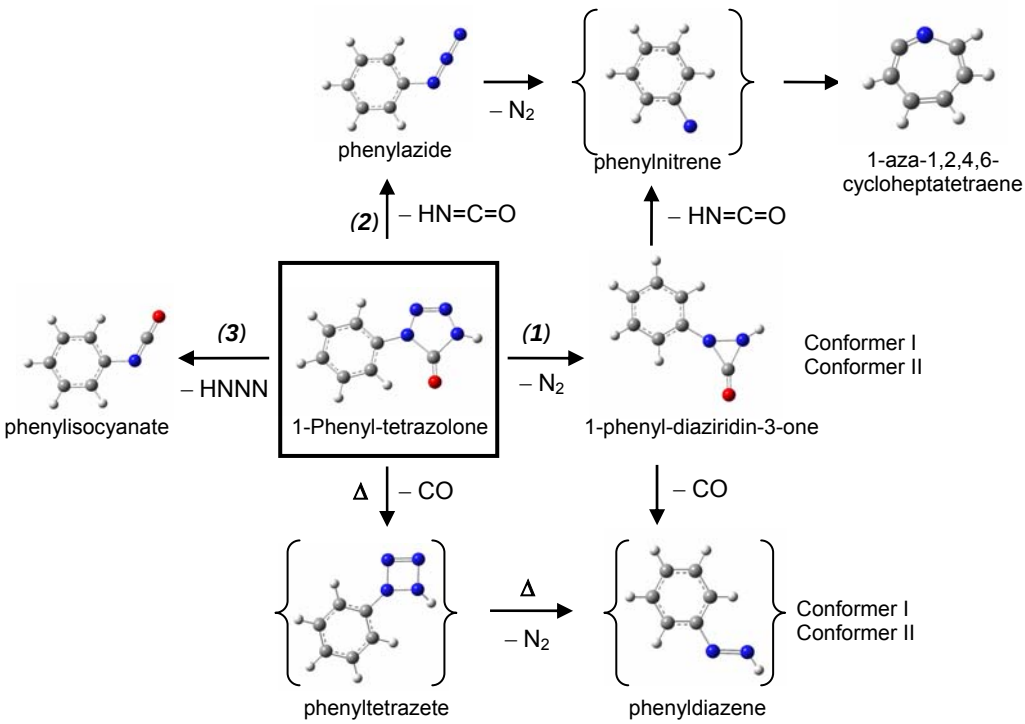


**Figure 3.** Proposed pathways resulting from irradiation of monomeric 1-phenyl-tetrazolone (PT) isolated in an argon matrix through the outer KBr window of the cryostat ($\lambda > 235$ nm). The proposed pathway corresponding to the preferred gas-phase thermal (**Δ**) fragmentation is also indicated.

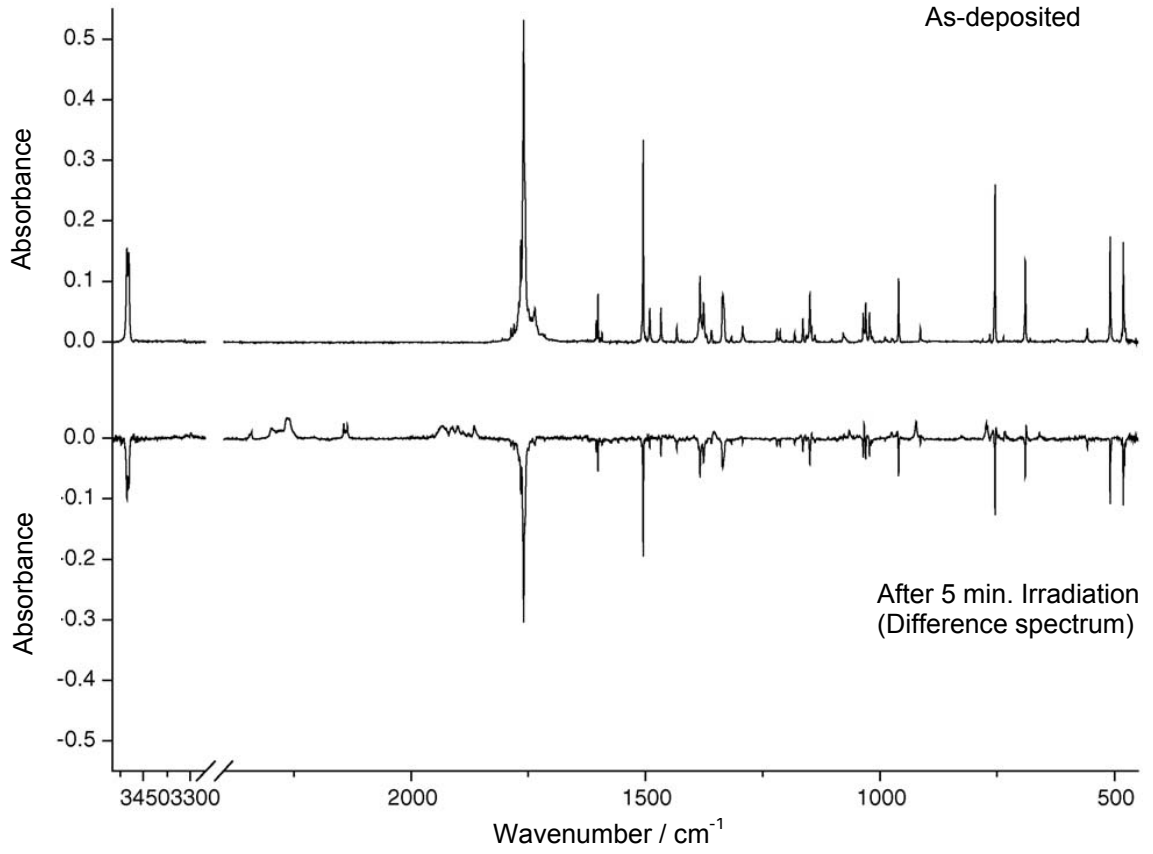


**Figure 4.** Infrared spectra of PT isolated in an argon matrix (as-deposited matrix) and after 5 min of irradiation ($\lambda$ > 235 nm) through the outer KBr window of the cryostat (difference spectrum: irradiated matrix minus as-deposited matrix).

Very interestingly, these photochemical reactions are distinct from the main thermal fragmentation reaction of PT, where CO is produced. Indeed, heating of the compound in the gas phase, prior to deposition of the matrix, led to appearance in the spectrum of the deposited gas of the characteristic narrow band of monomeric carbon monoxide, at 2135 $cm^{-1}$. Together with CO, the main thermal reaction leads to products that are weak IR absorbant species, since no other bands due to products of thermal fragmentation of PT could be identified in the spectra (there is also spectroscopic evidence of thermal production of a minor amount of phenylisocyanate, through observation of a weak band at the expected position of the intrinsically very intense band-mark of this compound, near 2260 $cm^{-1}$. However, taking into consideration the calculated relative intensities for this band, 1757 km $mol^{-1}$, and for the CO band, 89.2 km $mol^{-1}$, and the experimentally observed intensity ratio, *ca.* ½, this must correspond

to a much less efficient reaction channel for thermal fragmentation of PT). Both 1-phenyl-1,2-dihydrotetrazete and phenyldiazene, which can be obtained from 1-phenyl-1,2-dihydrotetrazete by molecular nitrogen elimination, satisfy the criterion of being weak IR absorbants [see Tables S5 and S16 (Appendix D)]. It can then be proposed that the preferred thermal fragmentation channel of PT consists in direct elimination of CO, with production of 1-phenyl-1,2-dihydrotetrazete, which quickly eliminates $N_2$, yielding phenyldiazene as the final product.

Photochemical *Pathway* 1 in PT corresponds to a molecular nitrogen elimination reaction, which leads to production of two conformers of 1-phenyl-diaziridin-3-one (I and II). The calculations predict these two conformers separated by 14.5 kJ $mol^{-1}$, with form (I) corresponding to the conformational ground state. In this form, the phenyl group and the diaziridinone-ring hydrogen atom are *trans* to each other (CCNC and O=C–NH dihedral angles equal to 41.6 and –90.5°). In conformer II (*cis*), these angles are 36.2 and 77.2°, respectively. The most intense bands of the diaziridinone isomers correspond to the νC=O and νC–N antisymmetric stretching vibrations and the γ(C–H ring 1) rocking mode. All the bands corresponding to these vibrations could be identified in the spectra: for conformer I, they are observed at 1931.9/1926.0/1877.8/1874.3 (site-split Fermi resonance doublet resulting from interaction of νC=O with the νC–N first overtone), 964.5/962.8 (νC–N) and 771.0 $cm^{-1}$ [γ(C–H ring 1)] (calculated values: 1931.2, 945.5 and 756.2 $cm^{-1}$), while for conformer II the corresponding bands are observed at 1913.1/1899.4/1865.8/1862.7, 924.0/922.8 and 695.3 $cm^{-1}$ (calculated values: 1921.2, 910.0 and 694.2 $cm^{-1}$). Other theoretically predicted intense bands of the diaziridinone could also be observed in other spectral regions, corresponding to a total of 22 different experimentally observed vibrations (see Table 2).

The bands due to the diaziridinone were in fact relatively easy to identify, since they only increased of intensity during the first half of the irradiation time (*i.e.*, until *ca.* 30 min of irradiation; in fact, the bands due to the less stable conformer start to decrease before this time). Indeed, this is the only directly observable product whose bands exhibit this behavior, which is consistent with the fact that this compound can further react during irradiation in a significant extent and with a rate constant of the same order of magnitude of that associated with the reaction leading to its formation. Two different pathways can be postulated for photodegradation of the diaziridinone, the first one yielding phenyldiazene plus CO, and the second one leading to production of phenylnitrene and isocyanic acid (with the nitrene undergoing subsequent ring expansion to 1-aza-1,2,4,6-cycloheptatetraene[27-29]). The characteristic behavior of the intensity changes with time of irradiation noticed for the bands ascribed to the diaziridinone is especially evident in the νC=O region, where the bands ascribed to this species were shown only to increase of intensity in the first 30 min of irradiation, while the bands observed in the same spectral region at 1894.2 and 1889.8 $cm^{-1}$, ascribed to 1-aza-1,2,4,6-cycloheptatetraene, show a continuous growth even for longer irradiation times (Figure 5). A CO elimination reaction from the diaziridinone would lead to simultaneous production of phenyldiazene, and it could be expected that these two species would interact with each other in the matrix cage where they are formed. Then, the photochemically formed associated CO should absorb at different frequency, when compared with the isolated monomer. In fact, while the characteristic band of the isolated CO monomer observed in the as-deposited matrix as result of thermal degradation in the gas phase prior to deposition did not increase during the irradiation of the matrix, other features were observed to grow in this spectral region (as expected for associated CO), appearing at higher frequencies and being considerably broader.[25]

**Table 2.** Experimental and calculated [DFT/B3LYP/6-311++G(d,p)] frequencies and intensities of the observed photoproducts of PT.[a]

| Molecule | Calculated | | Observed frequency ($cm^{-1}$) | | Approximate Description[c] |
|---|---|---|---|---|---|
| | Frequency ($cm^{-1}$) | Intensity (km $mol^{-1}$) | Reference[b] | This study | |
| 1-Phenyl-diarizirin-3-one | | | | | |
| I | 3390.5 | 31.8 | | 3299.0 | νN–H |
| II | 3296.9 | 9.1 | | 3241.9/3214.9 | νN–H |
| I | 1931.2 | 669.7 | | 1931.9/1926.0 | νC=O FR 2xν C–N *as*. |
| | | | | 1877.8/1874.3 | |
| II | 1921.2 | 645.7 | | 1913.1/1899.4 | νC=O FR 2xν C–N *as*. |
| | | | | 1865.8/1862.7 | |
| I | 1599.2 | 18.1 | | 1589.9 | ν(C–C ring 2) |
| II | 1597.2 | 12.9 | | 1589.9 | ν(C–C ring 2) |
| I | 1486.4 | 36.2 | | 1488.3 | δC–H ring 2) |
| II | 1484.1 | 34.2 | | 1488.3 | δ(C–H ring 2) |
| II | 1242.9 | 48.8 | | 1240.9 | νN–C (inter-ring) |
| I | 1236.2 | 54.1 | | 1237.9 | νN–C (inter-ring) |
| I | 1126.8 | 18.4 | | 1111.0 | δNH |
| I | 1078·6 | 5.6 | | 1075.8 | δ(C–H ring 3) |
| II | 1077.6 | 10.0 | | 1075.8 | δNH |
| I | 1066.3 | 30.9 | | 1063.9 | wNH |
| II | 1050.1 | 10.2 | | 1047.8 | wNH |
| II | 1041.4 | 19.6 | | 1043.6 | δ(C–H ring 3) |
| I | 945.5 | 140.1 | | 964.5/962.8 | νC–N *as*. |
| II | 915.6 | 61.4 | | 927.9 | γ(C–H ring 3) |
| II | 910.0 | 109.8 | | 924.0/922.8 | νC–N *as*. |
| I | 903.9 | 19.6 | | 912.3 | γ(C–H ring 3) |
| II | 762.3 | 45.9 | | 772.9/772.6 | γ(C–H ring 2) |
| I | 762.1 | 43.4 | | 772.9/772.6 | δ(ring 3) |
| II | 758.7 | 0.8 | | n.o. | δ(ring 3) |
| I | 756.2 | 51.9 | | 771.0 | γ(C–H ring 1) |
| II | 694.2 | 55.2 | | 695.3 | γ(C–H ring 1) |
| I | 691·8 | 24·1 | | n.o.[d] | γ(C–H ring 2) |
| I | 585.3 | 18.7 | | 583.5[e] | γC=O |
| II | 536.9 | 18.1 | | 543.3 | γC=O |
| Isocyanic acid | | | | | |
| | 2286.6 | 994.0 | 2259 | ≈2263[f] | νNCO *as*. |
| | 849.8 | 297.3 | 770 | 823.8 | δNH |
| | 626.8 | 21.5 | 573 | 629.8 | γNCO |
| Azide | | | | | |
| | 3398.1 | 94.1 | 3317 | 3313.9/3307.9 | νNH |
| | 2214.5 | 279.9 | 2135 | 2143.7/2139.6/2137.8[g] | $\nu N=N^{+}=N^{-}$ *as*. |
| | 1277.3 | 9.1 | 1263 | 1278.6/1266.9 | $\nu N=N^{+}=N^{-}$ *s*. |
| | 1166.9 | 267.8 | 1146 | 1169.4/1159.7/1154.1 | δNH |
| | 523.5 | 22.3 | 533 | 537.2[h] | $\gamma N=N^{+}=N^{-}$ |
| Phenylazide | 2197.1 | 772.6 | 2165/2157/2137 2128/2112/2102 2087 | 2143.7/2139.6/2137.8[g] | $\nu N=N^{+}=N^{-}$ *as*. |
| | 1600.2 | 47.4 | 1598 | 1597.0 | ν(C–C ring 2) |

**Table 2 (Continued)**[a]

| | | | | | |
|---|---|---|---|---|---|
| | 1488.8 | 72.6 | 1496/1491 | 1457.7 | δ(C–H ring 2) |
| | 1315.3 | 147.9 | 1398 | 1349.2 | νN $=N^{+}=N^{-}$ *s*. |
| | 1309.0 | 13.9 | 1337 | 1311.2 | δ(C–H ring 1) |
| | 1299.0 | 32.2 | 1305/1298 | 1296.5 | ν(C–C ring 3) |
| | 1129.3 | 26.3 | 1136/1131 | 1130.2 | νC–N |
| | 1085.2 | 8.6 | 1076 | 1075.8 | δ(C–H ring 3) |
| | 810.3 | 43.5 | 810 | 801.9 | δCNN |
| | 747.2 | 68.7 | 751 | 733.9 | γ(C–H ring 1) |
| | 683.6 | 26.6 | 687 | 660.7 | τ(ring 1) |
| | 670.7 | 26.7 | 670 | 652.6 | δN$=N^{+}=N^{-}$ |
| | 509.6 | 15.4 | 537 | 537.2[h] | γN $=N^{+}=N^{-}$ |
| 1-Aza-1,2,4,6-cycloheptatetraene | | | | | |
| | 1913.1 | 202.2 | 1895 | 1894.2/1889.8 | νC=C=N *as*. |
| | 1339.8 | 19.8 | 1348 | 1349.0 | δ(CH 1) |
| | 1301.5 | 3.0 | 1303.4 | ν C=C=N *s*. | |
| | 1110.9 | 15.2 | 1111/1105 | 1111.0/1104.9[i] | δ(CH 2) |
| | 979.7 | 25.6 | 980 | 975.5 | νNC |
| | 951.4 | 3.0 | 952.2 | γ (CH 1) | |
| | 945.7 | 4.5 | 940 | 942.2 | γ(CH 2) |
| | 850.6 | 4.7 | 860.6 | δ (ring 1) | |
| | 823.2 | 2.6 | 823.8 | δ (ring 2) | |
| | 754.3 | 62.3 | 748 | 758.7 | γ(CH 3) |
| | 685.0 | 45.5 | 683 | 687.6 | δC=C=N |
| | 663.8 | 28.2 | 658/650 | 660.7 | τ(ring) |
| | 595.5 | 10.9 | 580 | 583.5[e] | γC=C=N |
| Phenylisocyanate | | | | | |
| | 2322.0 | 1839.7 | ≈2296/2289/2266 ≈2230 | 2296.8/2291.9/2283.5 2276.5/2267.1/2263.1 2260.6/2251.5/2231.3 2229.5/2207.2 | νNCO *as*. |
| | 1602.3 1518.6 | 44.4 | | n.o.[j] | ν(C–C ring 2) |
| | 1452.4 | 31.9 | | 1516.8 | νNCO *s*. |
| | | 10.3 | | 1441.2 | ν(C–C ring 6) |
| | 1290.7 | 4.8 | | 1289.5/1285.1 | ν(C–C ring 3) |
| | 1116.2 | 52.5 | | 1111.0/1104.9[i] | νC–N |
| | 1078.0 | 9.7 | | 1064.5 | δ(C–H ring 3) |
| | 904.3 | 5.7 | | n.o.[k] | γ(C–H ring 3) |
| | 750.9 | 63.7 | | 752.5 | γ(C–H ring 1) |
| | 750.1 | 13.2 | | 747.8 | δ(ring 3) |
| | 685.4 | 27.3 | | 687.6 | τ(ring 1) |
| | 623.7 | 26.4 | | 629.8 | δNCO |
| | 556.0 | 25.1 | | 583.5[e] | γNCO |

a Only data for bands that could be observed are presented (in two exceptional cases, calculated data is given for non-observed (n.o.) bands: for predicted intense bands that are overlapped by reactant bands and, for 1-phenyl-diarizirin-3-one, in the cases where the band due to the same vibration is observed for the other conformer). The full list of calculated frequencies and intensities is provided in Tables S4-S17 (Appendix D).

b Reference data: isocyanic acid,[30], azide,[31] phenylazide ,[28] 1-aza-1,2,4,6-cyclohepta-tetraene,[27] phenylisocyanate[32]. All data in argon matrix, except for phenyl azide ($N_2$ matrix).

c ν, stretching; δ, bending; γ, rocking (out of plane bending); τ, torsion; FR, Fermi resonance.

d Overlapped with the 756.1/754.6/752.2 $cm^{-1}$ multiplet band of PT.

e This band has partial contributions from several photoproducts.

f Buried under the intense group of bands due to νNCO *as.* of phenylisocyanate.

g This group of bands is assigned to both azide and phenylazide, since it was not possible to discriminate bands due to each individual molecule (see also text).

h This band has partial contributions at least from azide and phenylazide.

i Assigned to 1-aza-1,2,4,6-cyclohepta-tetraene, phenylisocyanate and 1-phenyl-diarizirin-3-one (I).

j Overlapped with the 1605.6/1601.6 $cm^{-1}$ bands of PT.

k Overlapped with the 914.2 $cm^{-1}$ band of PT.

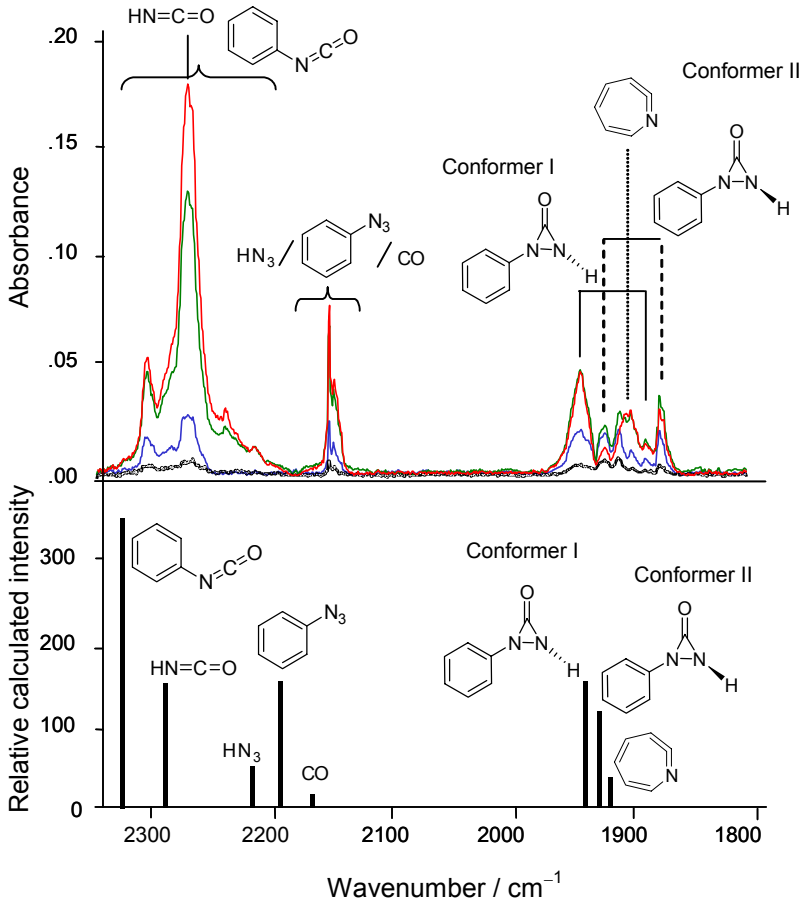


**Figure 5.** 2350–1800 $cm^{-1}$ spectral region of the irradiated ($\lambda$ > 235 nm) sample at different times of irradiation and calculated spectra, in this spectral range, for CO, azide, isocyanic acid, phenylazide, phenylisocyanate, 1-phenyl-diaziridin-3-one conformers (I and II) and 1-aza-1,2,4,6-cycloheptatetraene. Experimental spectra were obtained after 2 (black line), 10 (blue line), 30 (green line) and 60 (red dotted) min. of irradiation. Calculated spectra were obtained at the B3LYP/6-31++G(d,p) level of theory and simulated using Gaussian functions centered at the calculated (scaled) frequency and with bandwidth at half height equal to 5 $cm^{-1}$.

However, azides formed in *Pathways* 2 and 3 described below also absorb in this spectral region, and then the photoproduction of CO from the diaziridinone cannot be established with certainty from the analysis of this spectral region. Moreover, very unfortunately, according to the calculations the compound formed together with CO, phenyldiazene, does not have any strong IR band lying in a clean spectral region [in both possible conformations – see Table S5 (Appendix D)]. This fact precludes the direct experimental identification of this compound. However, methyldiazene (together with CS) has been previously identified as photoproduct of 1-methyl-1*H*-diazirene-3-

thiol subjected to identical experimental conditions[22] and, thus, the photochemical production of phenyldiazene (and CO) in the present case seems very likely.

The second process where the diaziridinone acts as reactant leads to production of isocyanic acid and phenylnitrene. The photochemistry of singlet phenylnitrene is well known.[27-29,33,34] It easily undergoes ring expansion to 1-aza-1,2,4,6-cycloheptatetraene [the calculated ground state energies for these two species favor the latter compound by *ca.* 80 kJ mol$^{-1}$ − see Tables S9 and S11 (Appendix D)], whose characteristic bands[33-34] could be clearly identified in the spectra of the irradiated PT Ar-matrix. Particularly noticeable is the intense band-mark associated with the antisymmetric stretching of the ketenimine moiety (νC=C=N *as.*) of 1-aza-1,2,4,6-cycloheptatetraene, observed at *ca.* 1895 cm$^{-1}$,[33] but other bands previously described by Huisgen et al.[34] as fingerprints of 1-aza-1,2,4,6-cycloheptatetraene could also be clearly identified in the spectra (Table 2), unequivocally testifying the photoproduction of this species. On the other hand, experimental identification of isocyanic acid is less straightforward, since the most intense bands of this compound[30,35-37] are nearly coincident with bands due to other photoproducts (see Table 2), in particular phenylisocyanate, which is formed in *Pathway 3* (Figure 3) and, as shown below, is one of the major observed photoproducts.

*Pathway 2* represents cleavage of the tetrazole ring to give isocyanic acid and phenylazide. This is then an alternative path for production of isocyanic acid to that discussed above and, with all probability, it shall correspond to the dominant reaction channel leading to this product. Phenylazide can further react, eliminating molecular nitrogen, to give phenylnitrene and then, again 1-aza-1,2,4,6-cycloheptatetraene. Phenylazide has been previously isolated and irradiated in both argon and nitrogen matrices, and production of 1-aza-1,2,4,6-cycloheptatetraene unequivocally demonstrated.[27-29] The vibrational spectrum of matrix-isolated phenylazide is well

known and its identification could be made here without any difficulty (see Table 2), despite the fact that, in the present case, phenylazide can be expected to interact with isocyanic acid produced in the same matrix cage [see Figure 6 for the calculated minimum energy structure of the phenylazide / isocyanic acid associate, and Table S17 (Appendix D), for the complete calculated IR spectrum of this species]; the associate is a planar species, with the isocyanic acid hydrogen pointing to the nitrogen atom of phenylazide connected to the phenyl ring and one of the *ortho* hydrogen atoms of the phenyl ring of this latter molecule pointing to the nitrogen atom of isocyanic acid.

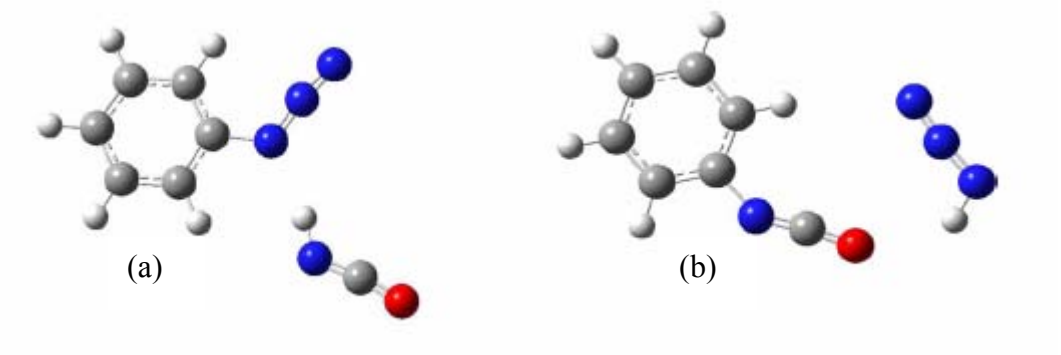


**Figure 6.** Calculated B3LYP/6-31++G(d,p) minimum energy structures of (a) phenylazide/isocyanic acid and (b) azide/phenylisocyanate complexes.

The associate has then two hydrogen-bond like interactions with calculated NH···N and CH···N distances of 205.1 and 295.4 pm, respectively. Since the bands assigned to phenylazide still continue to grow after 60 min. of irradiation, it can be concluded that, under the experimental conditions used, phenylazide reacts with relatively low efficiency, in particular when compared to PT, being formed faster than it is consumed to yield 1-aza-1,2,4,6-cycloheptatetraene (note that the amount of this latter compound formed cannot be used to estimate relative efficiencies of the different processes because it can also be produced in *Pathway* 1).

As already noticed, phenylnitrene (in triplet state) could also be previously observed in low temperature matrices as a result of direct photolysis of isolated

phenylazide.[29] However, we have no convincing evidence pointing to a direct experimental observation of this species in our spectroscopic data, even when irradiation was undertaken using different wavelength cut-off filters (*e.g.*, 285, 337, 375 and 417 nm). As for other molecules studied in this research project, the absence of observation of triplet phenylnitrene in the present study may result from the fact that phenylazide and isocyanic acid are produced together and interact in the matrix cage, eventually making inaccessible the pathway that would lead to formation of the triplet phenylnitrene (or, alternatively, favoring its fast decay, once formed, to the reactive singlet state).

*Pathway* 3 corresponds to tetrazole ring-opening leading to phenylisocyanate and azide as photoproducts (see Figure 3). There is no indication that these compounds undergo additional reactions. On the other hand, being produced in the same matrix cage they can interact with each other leading to formation of a phenylisocyanate/azide associate. We have undertaken extensive calculations on this associate and found only one minimum in its potential energy surface (double-degenerated by symmetry). The minimum energy structure is depicted in Figure 6. It is a planar species, with the hydrogen of the azide pointing to the oxygen atom of the phenylisocyanate and one of the *ortho* hydrogen atoms of the phenyl ring of this latter molecule pointing to the terminal nitrogen atom of the azide. The associate has then two hydrogen bonds (NH···O and CH···N distances are calculated as 232.7 and 297.8 pm, respectively), which form a 10-membered ring. The calculated stabilization energy (including zero point energy correction) due to formation of the associate amounts to -10.10 kJ $mol^{-1}$.

The spectrum of the matrix-isolated azide has been reported previously.[31,38-41] Himmel et al.[31] described signals at 3317, 2135, 1263, 1146 and 533 $cm^{-1}$ as fingerprints of azide. In the present study, all these bands were identified, though as

shown in Table 2, they appear at slightly different frequencies, with all probability as a consequence of the interaction of azide with phenylisocyanate. On the other hand, Pritchina et al.[32] have reported the spectrum of phenylisocyanate in solid argon, which in that case resulted from photolysis of benzoylazide. The experimental spectrum of phenylisocyanate is easily identifiable because it shows a very intense multiplet in the 2290–2260 $cm^{-1}$ region, due to the νNCO antisymmetric stretching vibration, that clearly dominates the spectrum. According to the theoretical predictions, the intensity of such unusually intense band represents about 90% of the total intensity of the spectrum of phenylisocyanate [see Tables S13 and S15 (Appendix D)].

It is worth to point out that, as mentioned before, the ν(NCO) asymmetric stretching of isocyanic acid is also expected to absorb in this spectral region. However, reaction *Pathway 3* appears to be the dominant one and phenylisocyanate shall thus be produced in a relatively larger amount than isocyanic acid. Besides, the predicted IR intensity for the ν(NCO) asymmetric stretching in phenylisocyanate is by far larger than in isocyanic acid (1840 km $mol^{-1}$ versus 994 km $mol^{-1}$). In view of these data, it can confidently be stated that the profile of the complex band in the 2290–2260 $cm^{-1}$ region is essentially due to the absorption of phenylisocyanate. Detailed analysis of the band as a function of the time of irradiation shows that the component at 2263 $cm^{-1}$ follows a slightly different pattern of variation (Figure 5) pointing to an additional contribution to this wavenumber of an absorption from other photoproduct, which cannot be other than isocyanic acid (this wavenumber closely matches the previously reported one for matrix-isolated isocyanic acid: 2259 $cm^{-1}$).[30]

The νNCO antisymmetric stretching vibration is strongly involved in Fermi resonance interactions, whose profile was found to closely follow that observed for the isolated phenylisocyanate monomer[32] (see Table 2). This means that the interaction

between phenylisocyanate and azide in the associate is not strong enough to introduce dramatic changes in the vibrational potential of phenylisocyanate. Support to this conclusion can also be found by comparing the spectrum of the azide / phenylisocyanate complex [Table S15 (Appendix D)] with that of the free phenylisocyanate monomer shown in Table S13 (Appendix D): the average relative shift in the band maximum wavenumbers upon complexation is as low as 0.86%.

Other less intense bands, appearing in the 1550–550 $cm^{-1}$ range, could also be assigned to phenylisocyanate, all of them correlating well with both the calculated spectrum for the azide/phenylisocyanate complex and the experimental data reported by Pritchina et al.[32] (see Table 2).

It is worth noticing that UV-irradiation of isocyanates (and also isothiocyanates), has been reported to induce partial isomerization to the corresponding cyanates (thiocyanates).[42-46] We tried then to found any experimental evidence of phenylcyanate and cyanic acid in the spectra of the irradiated matrices. However, we were unable to identify a band that could be unequivocally ascribed only to one of these molecules, which seems to indicate that they were not formed (at least in detectable amounts). In the case of cyanic acid, the absence of any band that could be assigned to the νOH stretching vibration (which, in the present case, should appear in a clean spectral region) is a strong indication of the absence of this species in the matrix.

A final note shall be made relatively to the energetic of the primary photochemical processes. Besides irradiation at $\lambda > 235$ nm, experiments were made with less energetic radiation, using different cut-off filters, from $\lambda > 417$ nm to $\lambda > 285$ nm. Under all these conditions, the compound was found to be photostable. The minimum energy required to trigger the photochemistry of PT was shown to be within the 284 nm – 235 nm (*i.e.*, 420–510 kJ $mol^{-1}$) range. Such range of energies is in the

same order of magnitude of the sum of bond energies typical of C–N and N–N bonds (276 and 193 kJ $mol^{-1}$, respectively)[47].

## ▪ Conclusions

The structure, vibrational properties and photochemistry ($\lambda$ > 235 nm) of 1-phenyl-tetrazolone have been studied, for the compound isolated in solid argon. It was found that only one tautomer of this molecule (1-phenyl-1,4-dihydro-5*H*-tetrazol-5-one) contributes to the spectrum of the as-deposited matrix, indicating that, in the gaseous phase, only this tautomer exists. After UV-irradiation of the matrix, three different pathways could be identified, all of them corresponding to cleavage of the tetrazole ring. The identification of the photoproducts was carried out taking into account both the DFT/B3LYP/6-311++G(d,p) calculated spectra for different putative products and the available literature data on those compounds. The following primary photoproducts could be identified in the matrices after irradiation: *Pathway* 1: two conformers of 1-phenyl-diaziridin-3-one; *Pathway* 2: phenylazide and isocyanic acid; *Pathway* 3: azide and phenylisocyanate. Secondary products resulting from *Pathways* 1 and 2 could also be identified: these are 1-aza-1,2,4,6-cycloheptatetraene and associated carbon monoxide. The additional production of cyanic acid and phenyl cyanate by isomerization of isocyanic acid and phenylisocyanate looks improbable under the experimental conditions used. The observed photochemical processes are distinct from the preferred thermal fragmentation channel, where CO is produced together with a weak IR absorbant species, with all probability phenyldiazene (with 1-phenyl-1,2-dihydrotetrazete as possible intermediate).

## 3.3.3. UV-induced Photochemistry of Matrix-isolated 1-Phenyl-4-allyl-tetrazolone

- Molecular geometry and infrared spectrum of the matrix-isolated compound (as-deposited matrix)

The geometry optimizations carried out for 1-phenyl-4-allyl-tetrazolone (PAT), led to the identification of three low energy local minima, corresponding to the structures Sk' ("Skew-minus"), Sk ("Skew-plus") and Syn, represented as Newman projections in Figure 7 [for optimized geometries see Tables S19-S21 (Appendix D)]. All these minima depend on the position of the ethene group on the allylic chain attached to the tetrazole ring, and their structures result from rotation of this group around the $C_{(7)}$–$C_{(8)}$ bond in PAT. The potential energy profile for this internal rotation (Figure 7) was calculated by incrementing the value of the $N_{(4)}$–$C_{(7)}$–$C_{(8)}$=$C_{(9)}$ dihedral angle and fully optimizing all other geometric parameters. The three low energy conformers Sk', Sk and Syn have very close relative energies, which fall in the 0 – 2.3 kJ $mol^{-1}$ range (see Figure 7). At the B3LYP/6-311++G(d,p) level, the relative energies of Sk', Sk and Syn were calculated to be 0, 0.2 and 2.2 kJ $mol^{-1}$, respectively (ZPVE corrections included). The small differences in the energy of conformers can be explained considering interactions between the allylic chain and the tetrazole ring of PAT. In conformer Sk' (the lowest energy structure) the ethene group on the allylic chain is as far as possible from the tetrazole ring and opposite to the carbonyl oxygen $O_{(6)}$, which minimises repulsive interactions in the molecule and consequently its energy. Also, in conformer Sk the ethene group on the allylic chain remains distant from the tetrazole ring, but the closer proximity of the ethene group to the oxygen atom is responsible for a slight increase in energy of Sk relatively to the Sk' form ($\Delta E$ = 0.2

kJ $mol^{-1}$). The structure Syn is the most unstable conformer among the three calculated minima, this fact being attributed to the spatial proximity between the ethene group and the tetrazole ring.

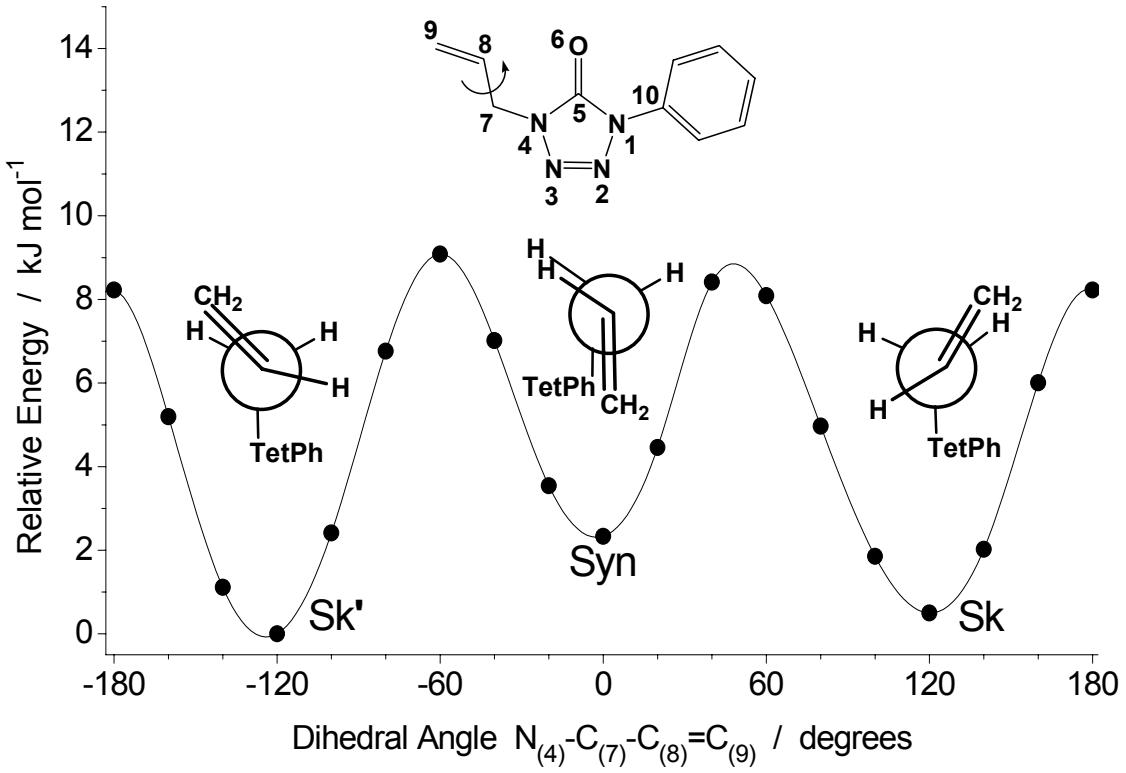


**Figure 7.** Relaxed potential energy scan for internal rotation of the ethene group around the $C_{(7)}$–$C_{(8)}$ bond in 1-phenyl-4-allyl-tetrazolone, calculated at the DFT(B3LYP)/6-31(d,p) level of theory. The reaction coordinate was incrementally fixed while all other geometrical parameters were fully optimized. Minima denoted as **Sk'**, **Syn** and **Sk** correspond to conformers "Skew-minus", Syn, "Skew-plus" and are represented as Newman projections. The lowest-energy structure is conformer **Sk'**. Its energy (-681.271842 hartrees) was chosen as the relative zero level.

Calculations show that in all conformers the phenyl and tetrazole rings have approximately planar geometries and are coplanar to each other. This last result can be mostly attributed to the favourable interactions between the phenyl hydrogen atoms *ortho* to the tetrazole ring, and the carbonyl oxygen and $N_{(2)}$ atoms, respectively (Figure 7). Structural data for the co-planar phenyl and tetrazolyl rings in PAT are similar to those observed for 1-phenyl-tetrazolone (PT).[48] On the other hand, also for all

conformers, the geometry around the $N_{(4)}$−$C_{(7)}$ bond has been found to be the same, with the $C_{(8)}H$=$C_{(9)}H_2$ fragment being perpendicular to the tetrazolone ring.

Because of the small energy differences between the three forms, it can be expected that all of them are present in the gas phase in significant amounts. Indeed, at 77°C, the predicted populations of forms Sk', Sk and Syn are 41.8%, 38.8% and 19.4%, respectively. The energy barriers separating these forms were predicted to be higher than 8 kJ $mol^{-1}$ in both directions (calculated at the DFT(B3LYP)/6-31G(d,p) level of theory, see Figure 7). Although these barriers are not very high, they are related with rotation of a bulky −$CH_2$−CH=$CH_2$ group. The size of the group hinders its internal rotation in the rigid environment (low-temperature matrix) and precludes interconversions between the three conformers. This implies that the relative populations of the three conformers of PAT trapped into an Ar matrix should be the same as they were in the gas phase, prior to deposition.[49]

The experimental IR spectrum of PAT monomers, isolated in an Ar matrix, is presented in Figure 8 (*trace a*). This spectrum is well reproduced by the spectrum of a conformer mixture (*trace b*) simulated theoretically [at the DFT(B3LYP)/6-311++G(d,p) level, see Figure 8 (*trace b*)].

The calculated spectra of the three forms of PAT are very similar to each other [see Figure S1 (Appendix D)], making very difficult to distinguish these forms spectroscopically. Luckily, the precise knowledge concerning the conformational orientation of the allyl group (–$CH_2$–CH=$CH_2$) is not essential for the interpretation of photochemical transformations of PAT isolated in an argon matrix, as it will be shown below.

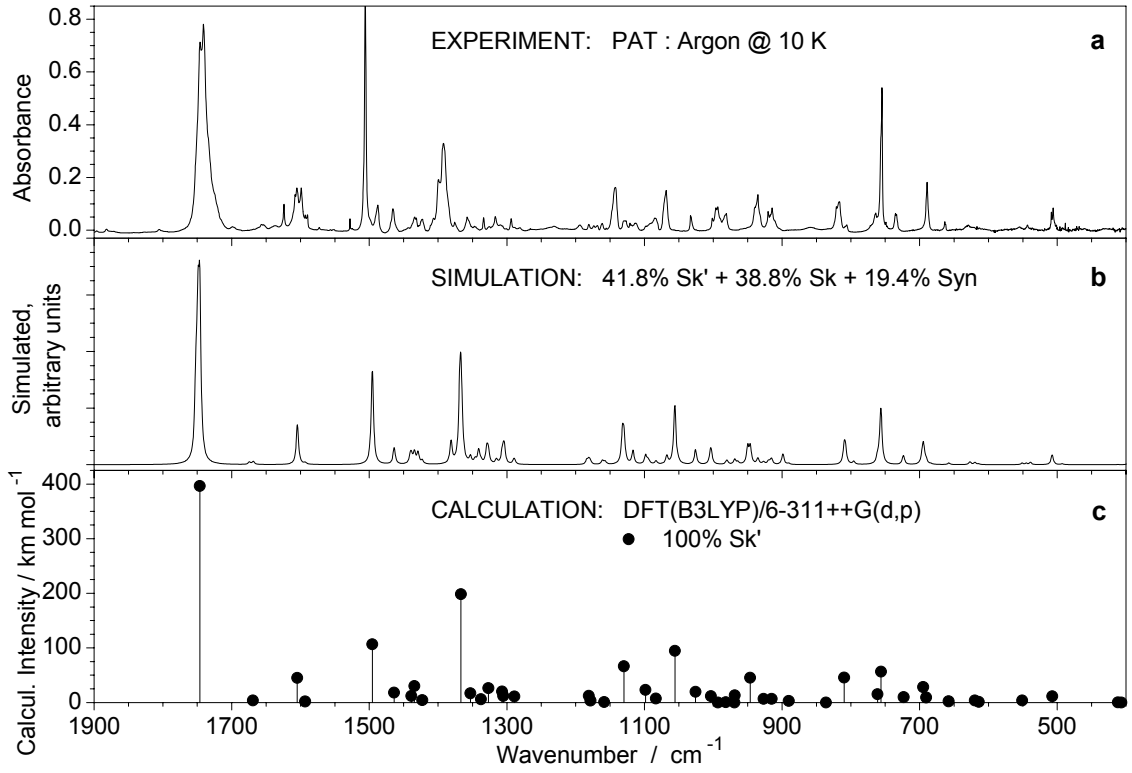


**Figure 8.** ***a)*** Experimental FTIR spectrum of monomeric 1-phenyl-4-allyl-tetrazolone (PAT) trapped in an argon matrix at 10 K, immediately after deposition; ***b)*** Infrared sum spectrum of the characteristic equilibrium mixture of PAT conformers at 77 °C. The spectra of individual conformers were simulated with Lorentzian functions centered at the calculated (scaled) frequencies and with bandwidths-at-half-height equal to 4 $cm^{-1}$. The calculated intensities of different conformers were population-weighted; ***c)*** DFT(B3LYP)/6-311++G(d,p) calculated infrared spectrum of the most stable conformer (Sk′). The calculated wavenumbers were scaled with a uniform factor of 0.978. The calculated intensities were not scaled. For simplicity, only the spectrum of the most stable form is shown, since the predicted spectra of all conformers are very similar. Spectra of individual conformers are provided in Table S18 (Appendix D).

## ▪ *In situ* UV-irradiation experiments (λ > 235 nm)

As mentioned above, the photochemistry in solution of a series of 4-allyl-tetrazolones, including PAT, was recently studied in our laboratory, revealing that the photolysis in alcoholic solutions leads to new heterocycles, namely 3,4-dihydro-pyrimidin-2(1*H*)-ones, in almost quantitative yields. In the specific case of PAT photolysis in alcoholic media led to exclusive formation of 3,4-dihydro-3-phenylpyrimidin-2(1*H*)-one (PDP, Figure 9). Results from a previous investigation carried out by Quast and co-workers, under different experimental conditions, indicated

that photolysis of PAT in solution leads to formation of 1-allyl-1*H*-benzoimidazol-2(3*H*)-one (ABZ, Figure 9) as the sole product.[50] Both primary photoproducts, PDP and ABZ, detected upon photolysis of PAT in solution, result from elimination of nitrogen from the tetrazole ring, followed by two distinct processes of cyclization. The different reactivity revealed in these two experiments can be attributed to changes of experimental forum, which clearly affect the reactivity and stability of the intermediate species involved. The divergent results obtained for the photolysis of PAT in solution, are indicative of the high sensitivity of this system to the characteristics of reaction media, made the photochemical investigation of this compound in cryogenic matrices an especially attractive challenge.

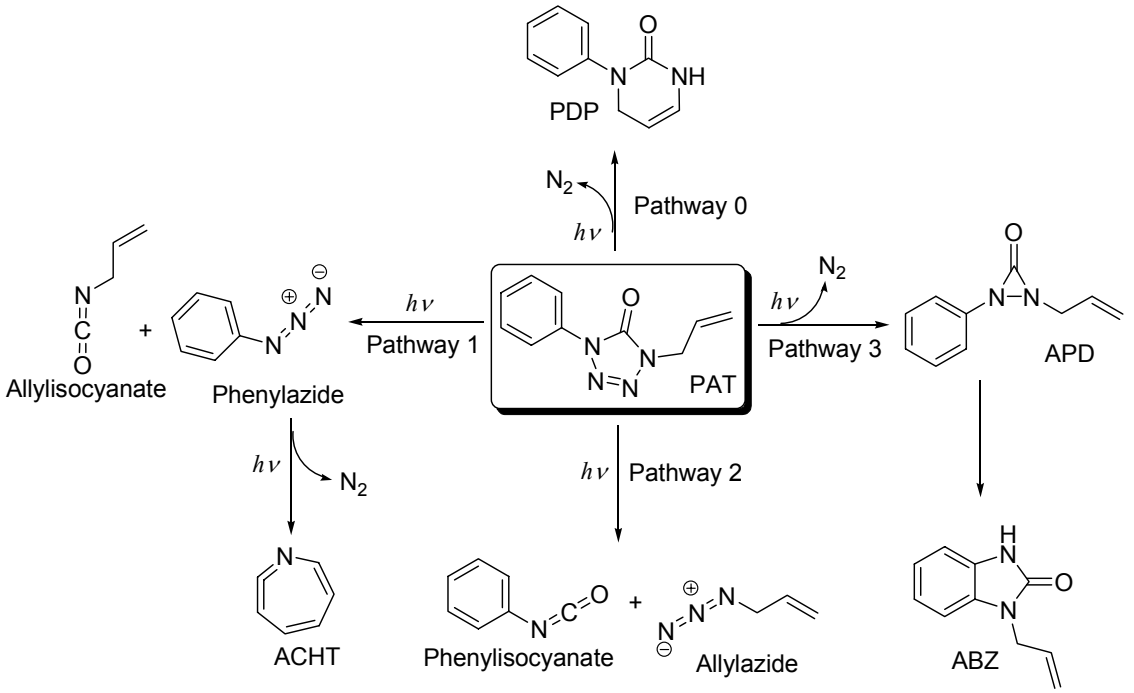


**Figure 9.** Proposed photochemical pathways resulting from irradiation of 1-phenyl-4-allyl-tetrazolone (PAT) in an argon matrix through the outer KBr window of the cryostat ($\lambda > 235$ nm).

To study the photochemistry of the matrix-isolated PAT, *in situ* UV-irradiation ($\lambda > 235$ nm) experiments were carried out. The resulting photochemical processes were followed by IR spectroscopy and the interpretation of the experimental

spectroscopic data was supported by extensive DFT calculations on plausible photoproducts, taking into consideration previously reported spectroscopic data, whenever available.

Upon UV-irradiation of matrix-isolated PAT, the intensities of the bands of this compound decreased significantly while new bands appeared in the infrared spectrum, indicating that the compound was transformed in diverse photoproducts. The changes are particularly evident in the 2300-1700 $cm^{-1}$ spectral region, which is shown in Figure 10 (part A). For the conformationally flexible photoproducts all conformational possibilities were explored (about one week of parallel calculations on several PC's). In the simulated spectra, only the most stable conformers for each photoproduct were considered (Figure 10). Further conformers were neglected in this analysis on the basis that their calculated spectra are very similar within the same photoproduct. The validity of such approach is demonstrated by a reasonable correspondence between the simulated and the observed spectra of photoproducts.

The possible reaction pathways proposed, resulting from irradiation of PAT, are schematically shown in Figure 9.

The photochemistry of the matrix-isolated compound reveals three main reaction pathways: *(1)* cleavage of the tetrazole ring through the formally single bonds $C_{(5)}–N_{(1)}$ and $N_{(3)}–N_{(4)}$, with production of phenylazide and allylisocyanate as primary photoproducts (phenylazide can then undergo additional reactions to give 1-aza-1,2,4,6-cycloheptatetraene); *(2)* cleavage of the $N_{(1)}–N_{(2)}$ and $C_{(5)}–N_{(4)}$ bonds, leading to formation of phenylisocyanate and allylazide; and *(3)* cleavage of the $N_{(1)}–N_{(2)}$ and $N_{(3)}–N_{(4)}$ bonds producing 1-allyl-2-phenyldiaziridin-3-one (APD). This compound is then partially transformed in 1-allyl-1*H*-benzoimidazol-2(3*H*)-one (ABZ).

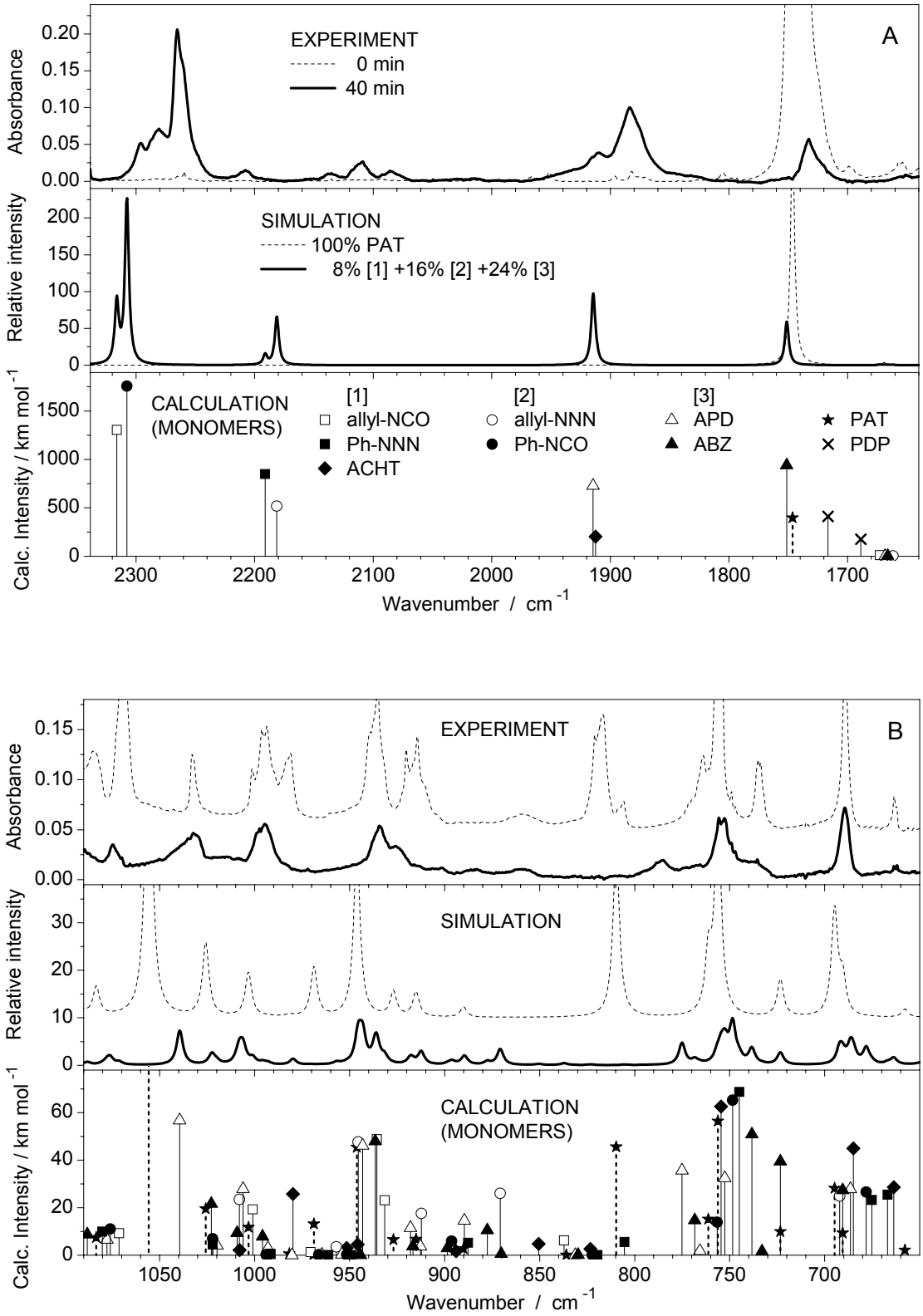


**Figure 10.** Infrared spectra of 1-phenyl-4-allyl-tetrazolone (PAT) and the proposed photoproducts, in the carbonyl stretching (A) and fingerprint (B) regions. (continued)

(**Figure 10. Continued**)
*Upper frames* (EXPERIMENT): dashed line - FTIR spectrum of monomeric PAT trapped in an argon matrix at 10 K immediately after deposition (0 minutes of irradiation); solid line - extracted spectrum of the photoproducts formed after 40 minutes of UV-irradiation ($\lambda$>235 nm) of PAT trapped in an Ar matrix. The extracted spectrum was obtained by subtraction of the scaled spectrum of non-irradiated matrix from the spectrum of irradiated sample. The scaling factor was chosen so that the absorptions due to the originally deposited compound (PAT) were nullified.
*Lower frames* (CALCULATION): DFT(B3LYP)/6-311++G(d,p) calculated spectra of PAT (dashed sticks) and possible photoproducts. The calculated wavenumbers were scaled with a uniform factor of 0.978. The calculated intensities were not scaled. Groups [1], [2] and [3] designate different photochannels.
*Middle frames* (SIMULATION): simulated infrared spectra of PAT (dashed line) and a mixture of photoproducts (solid line). They were created using Lorentzian functions centered at the calculated (scaled) frequencies (shown in the lower frames) and with bandwidths-at-half-height equal to 4 $cm^{-1}$. The calculated intensities in the spectrum of PAT were taken as 100%. The calculated intensities of photoproducts were scaled down to reproduce the relative intensities in the experimental spectrum of photoproducts in the carbonyl stretching region (part A) and to obey the normalization condition: total amount of photoproducts is equal to the amount of consumed reagent (48%).
Note that in the fingerprint region (part B), the experimental (upper frame) and simulated (middle frame) spectra of PAT (dashed lines) are shifted on ordinate for clarity. The symbols of PAT and photoproducts are the same in parts A and B.

The possible formation of PDP from PAT, shown by the *Pathway* "0" in Figure 9, was found not to occur under the present experimental conditions, contrarily to what was observed upon the photolysis of PAT in solution. The designation of *Pathway* "0" illustrates that the outcome of this channel in the argon matrix at 10 K is equal to 0%. The non-formation of PDP in this study is doubtlessly related with the matrix medium where this reaction pathway is suppressed. Very likely, a strong restriction of conformational mobility in the argon matrix affects not only PAT itself, but also its photoproducts. The formation of PDP from PAT (after extrusion of $N_2$) involves an approach between the terminal carbon of the allylic chain and the nitrogen atom $N_{(1)}$, in order to form a new C–N single bond. Such approach is strongly hindered in the rigid matrix, which consequently precludes formation of PDP. The inclusion of the hypothetic reaction channel leading to PDP in the general scheme presented in Figure 9 results from the initial assumption that this could be a possibility, in view of the results obtained in solution. For the sake of simplicity, the calculated spectrum of PDP is omitted in part B of Figure 10.

The observed photoprocesses in the argon matrix (*Pathways* 1 to 3 in Figure 9) result from cleavage of the four formally single bonds in different combinations, with every primary photoreaction involving cleavage of two single bonds in the tetrazole ring. After 40 minutes of UV-irradiation, the amount of the consumed reagent is equal to 48%. This percentage should then correspond to the sum of efficiencies of the three observed reaction pathways and to the total amount of photoproducts.

All strong and medium intensity bands calculated for the two primary photoproducts formed in *Pathway* 1 (phenylazide and allylisocyanate) could be observed in the spectra of the irradiated matrix (see Figure 10). The experimental spectrum of aliphatic isocyanates, such as allylisocyanate, is usually easily identifiable, because it shows an intense vibration in the 2290–2300 $cm^{-1}$ region due to the νN=C=O antisymmetric stretching vibration. In the spectrum of photoproducts (Figure 10A) the band associated to this vibration emerges at 2296.5 $cm^{-1}$, proving formation of allylisocyanate upon PAT photolysis.

*Pathway* 1 shows a secondary process resulting from conversion of phenylazide in 1-aza-1,2,4,6-cycloheptatetraene (ACHT). Phenylazide has been previously isolated and irradiated in an argon matrix, and its conversion into ACHT clearly demonstrated.[48] The vibrational spectra of matrix isolated phenylazide[51] and of ACHT are well known and their identification was made without any difficulty. In the spectrum of the photoproducts, the most prominent band of phenylazide appears at 2108.8 $cm^{-1}$ and is ascribed to the $\nu N=N^{+}=N^{-}$ antisymmetric stretching vibration. Characteristic bands of ACHT[48] were also clearly identified in the spectra of the irradiated matrix. Particularly evident is the band-mark associated with the intense antisymmetric stretching vibration of the ketenimine moiety (*ν*C=C=N as.) of ACHT, observed at 1910.5 $cm^{-1}$ (Figure 10).

The efficiencies of the different photochannels were estimated on the basis of the comparison between the relative band intensities for the photoproducts observed experimentally. These intensities were pre-normalized by the calculated intensities of the putative photoproducts, using the observed and calculated absorptions in the 1600-2400 $cm^{-1}$ spectral region (see Figure 10A). The subsequent normalization was carried out in order to bring the total efficiency of all photochannels to be equal to the amount of consumed reagent (i.e. 48% after 40 minutes). The validity of this normalization procedure was then confirmed in the fingerprint region of spectrum (see Figure 10, part B), which provided a very nice correspondence between the simulated (middle frame) and the observed (upper frame) spectra.

We found that the transformation of PAT into allylisocyanate and phenylazide proceeds with low efficiency. Allowing for 48% of consumed reagent, only 8% (i.e. 1/6) is attributed to the reaction *Pathway* 1. On the other hand, the secondary transformation of phenylazide into ACTH was carried out with relatively high efficiency. Three quarters of the 8% attributed to this reaction channel were converted into ACHT [(Ph-NNN 2%) + (ACHT, 6%) = 8%].

Reaction *Pathway* 2 depicted in Figure 9 corresponds to tetrazole ring-opening leading to allylazide and phenylisocyanate as photoproducts. In the experimental spectrum of the photoproducts, the band that appears at 2085.6 $cm^{-1}$, in close proximity to the corresponding band for phenylazide, is ascribed to the $\nu N=N^{+}=N^{-}$ antisymmetric stretching vibration of allylazide. The spectrum of phenylisocyanate in solid argon has been reported,[48] and is easily identifiable because it shows a very intense vibration in the 2290–2260 $cm^{-1}$ region, due to the N=C=O antisymmetric stretching, that dominates the spectrum. In the spectrum of photoproducts (Figure 10, part A) this vibration

emerges as a doublet at 2280.3/2265.3 $cm^{-1}$, clearly demonstrating the formation of phenylisocyanate.

The conversion of PAT into phenylisocyanate and allylazide proceeds with relatively high efficiency. Considering the total amount of consumed reagent (48%), 16% (i.e. 1/3) is attributed to the reaction *Pathway* 2. Moreover, there is no indication that the compounds formed in this channel undergo additional reactions.

Photochemical *Pathway* 3 in PAT corresponds to a molecular nitrogen elimination reaction, which leads to formation of a three-membered heterocyclic ring, namely the 1-allyl-2-phenyldiaziridin-3-one (APD) (see Figure 9). To the best of our knowledge, this species was never described before.

Diaziridinones can be easily identified because their most intense IR band, corresponding to a vibrational mode with dominant contributions from the *ν*C=O and *ν*C−N antisymmetric coordinates, occurs in a "clean" region of the spectrum (1900–1850 $cm^{-1}$). In the spectra of the irradiated matrix, the band corresponding to this vibrational mode was clearly identified at 1883.2 $cm^{-1}$ (Figure 10, part A), confirming the formation of APD upon PAT photolysis.

*Pathway* 3 shows a secondary process resulting from conversion of APD into 1-allyl-*1H*-benzoimidazol-2(*3H*)-one (ABZ). In the spectra of the photoproducts, the band that appears at 1735.2 $cm^{-1}$, overlapped with the doublet at 1746.0/1740.9 $cm^{-1}$ due to the *ν*C=O antisymmetric stretching vibration of PAT, is attributed to the similar vibration (*ν*C=O) in ABZ (Figure 10, part A). Alternative attributions/photoproducts for the band registered at 1735.2 $cm^{-1}$ were investigated, but all of them were rapidly discarded. The validity of this attribution is confirmed by a good correspondence between the simulated and the observed spectra of ABZ. Furthermore, it was found that the transformation of PAT in APD plus ABZ occurs with a high efficiency. Allowing

for the total amount of consumed reagent (48%), 24% is attributed to the reaction *Pathway* 3.

On the other hand, the secondary transformation of APD into ABZ was carried out with relatively low efficiency (from 24%, only 8% (i.e. 1/3) was converted in ABZ). APD has a high conformational mobility, but only part of conformers bear a favorable spatial orientation wherein the close proximity of the phenyl and imidazole rings is not affected by the position of allylic fragment, and ABZ formation is possible. The restriction of conformational mobility in the matrix can therefore justify the low yield observed for this secondary transformation.

Interestingly, the allylic chain is maintained unbroken during the irradiation process, indicating that under the experimental conditions used this unit is photochemically stable. Finally, considering the efficiencies of the different reaction channels discussed, a remarkable relationship between their values is detected. The sequence "0 : 8 : 16 : 24" (%), associated to the efficiencies of *Pathways "0"* to 3 respectively, can be related as "0 : 1 : 2 : 3" as a perfect and interesting sequence. This is certainly accidental, but still a good example of how Nature can be endless source of symbolic beauty!

## ▪ Conclusions

The photochemistry of the matrix-isolated 4-allyl-1-phenyl-tetrazolone (PAT) has been investigated. The structures of the initial compound and of the photoproducts were determined by infrared spectroscopy, supported by high-level quantum chemical calculations. The DFT(B3LYP)/6-311++G(d,p) calculations performed in this study predict that, in the gaseous phase, PAT should exist in three different conformers, depending on the position of the ethene group on the allylic chain attached to the tetrazole ring. The potential energy profile for internal rotation of the ethene group was

calculated, revealing that the energy barriers separating the three conformers are higher than 8 kJ $mol^{-1}$. These barriers are not very high, but they are related to rearrangements of a bulky allyl fragment which are unlikely to occur in the matrix and thus prevent interconversions between the three conformers. Consequently, the experimental spectrum of PAT closely matches the infrared sum spectrum of the equilibrium mixture of PAT conformers predicted theoretically, pointing to the existence of the three structures in the low-temperature matrix.

The exposure of matrix-isolated PAT to the UV ($\lambda$ > 235 nm) light has been shown to induce three different photochemical pathways: *Pathway* 1: production of phenylazide and allylisocyanate as primary photoproducts; *Pathway* 2: production of phenylisocyanate and allylazide; and *Pathway* 3*:* molecular nitrogen elimination, leading to formation of 1-allyl-2-phenyldiaziridin-3-one (APD). The primarily formed phenylazide (*Pathway* 1) and APD (*Pathway* 3) are partially converted into 1-aza-1,2,4,6-cycloheptatetraene (ACHT), and 1-allyl-1*H*-benzoimidazol-2(3*H*)-one (ABZ) respectively. Both the vibrational characterisation of APD and the observation of its infrared spectrum were carried out for the first time.

The non-observation of *Pathway "*0*"* and the low efficiency observed for the secondary process from *Pathway* 3, in the matrix, is indicative that photoreactions involving conformational mobility (very efficient in solution) are severely restricted, due to the low conformational mobility of the studied system in the matrix.

## 3.3.4. Experimental Section

**Equipment and experimental conditions.** All chemicals were used as purchased from Aldrich. Solvents for extraction and chromatography were of technical grade. When required, the solvents used in reactions were freshly distilled from appropriate drying agents before use. Analytical TLC was performed with Merck silica gel 60 $F_{254}$ plates. Melting points were recorded on a Stuart Scientific SMP3 melting point apparatus and are uncorrected. Mass spectra were obtained on a VG 7070E mass spectrometer by chemical ionization (CI, $NH_3$). $^1H$ NMR (400 MHz) spectra were obtained on a Bruker AM-400 spectrometer using TMS the internal reference ($\delta$ = 0.0 ppm).

**Infrared spectroscopy.** The IR spectra were obtained using a Mattson (Infinity 60AR Series) Fourier transform infrared spectrometer, equipped with a deuterated triglycine sulphate (DTGS) detector and a Ge/KBr beamsplitter, with 0.5 $cm^{-1}$ spectral resolution. In order to avoid interference from atmospheric $H_2O$ and $CO_2$, a stream of dry nitrogen continuously purged the optical path of the spectrometer. The compound was placed in a specially designed doubly thermostattable Knudsen cell,[52] whose compartments (sample container and valve nozzle) were kept at 380 K (for PT) or 350 K (for PAT) during deposition of the matrix. Matrices were prepared by co-deposition onto the CsI substrate of the cryostat cooled to 10 K of PT or PAT vapors coming out of the Knudsen cell, together with and a large excess of the matrix gas (argon N60, Air Liquide) coming from a separate line. All experiments were performed using an APD Cryogenics closed-cycle helium refrigeration system with a DE-202A expander.

Irradiation of the samples was carried out with a 150W xenon arc lamp (Osram XBO 150W/CR OFR), through the outer KBr window of the cryostat ($\lambda$ > 235 nm).

**Computational methodology.** The quantum chemical calculations of the stationary points were performed at the DFT level of theory, using the standard 6-311++G(d,p) basis set and the three-parameter density functional abbreviated as B3LYP, which includes Becke's gradient exchange correction[53] and the Lee, Yang, Parr correlation functional.[54] Potential energy scans were performed using the 6-31G(d,p) basis set. Geometrical parameters were optimized using the Geometry Direct Inversion of the Invariant Subspace (GDIIS) method.[55] Optimization of geometries was followed by calculation of the vibrational spectra at the same theory level. The nature of the obtained stationary points was checked through analysis of the corresponding Hessian matrix. A set of internal coordinates was defined, and the Cartesian force constants were transformed to the internal coordinate space, allowing ordinary normal-coordinate analysis as described by Schachtschneider,[56] by using the optimized geometries and harmonic force constants resulting from the DFT(B3LYP)/6-311++G(d,p) calculations.

The calculated harmonic frequencies (scaled with a factor of 0.978) were used to assist the analysis of the experimental spectra and to account for the zero-point vibrational energy (ZPVE) corrections. All calculations in this work were carried out using the Gaussian 03 program.[57]

**Synthesis of 1-phenyl-tetrazolones (PT and PAT).**

**1-Phenyl-tetrazolone (PT).** NaOH pallets (2.01 g; 50 mmol) were dissolved in water (50 mL) at room temperature. 5-Chloro-1-phenyl-1*H*-tetrazole (1.0 g; 5.55 mmol) in THF (10 mL) was added and the mixture was stirred overnight at 50°C. The reaction was monitored by TLC, using a mixture of DCM/hexane (5:1) as eluent. A cold solution of HCl 3M (10 mL) was added to the final mixture, and a white precipitate was formed. The precipitate (1-phenyl-tetrazolone) was filtered and the remaining organic product

extracted from the aqueous solution with a mixture of ethyl acetate/DCM (5:1) (3 × 50 mL). The combined organic extracts were dried ($Na_2SO_4$) and evaporated to dryness to give 1-phenyl-tetrazolone as white powder (0.35 g; 39% yield), mp 190-191°C. $^1H$ NMR ($CDCl_3$): δ 4.90 (1H, s, NH), 7.53-7.89 (5H, d) ppm; MS (CI, $NH_3$), *m*/*z* 180 $[M+NH_4]^+$.

**1-Phenyl-4-allyl-tetrazolone (PAT)** was synthesised as described before (see Chapter 2 - Part 1, Experimental Section).

## 3.3.5. References


1. Singh, H.; Chawla, A.S.; Kapoor, V.K.; Paul, D.; Malhotra, R.K. *Prog. Med. Chem.* **1980**, *17*, 151.
2. Shih, T.L.; Candelore, M. R.; Cascieri, M. A.; Chiu, S.-H. L.; Colwell Jr., L. F.; Deng, L.; Feeney, W.P.; Forrest, M.J.; Hom, G.J.; MacIntyre, D.E.; Miller, R.R.; Stearns, R.A.; Strader, C.D.; Tota, L.; Wyvratt, M.J.; Fisher, M.H.; Weber, A.E. *Bioorg. Med. Chem. Lett.* **1999**, *9*, 1251.
3. Mathvink, R.J.; Tolman, J.S.; Chitty, D.; Candelore, M.R.; Cascieri, M.A.; Colwell, Jr., L.F.; Deng, L.; Feeney, W.P.; Forrest, M.J.; Hom, G.J.; MacIntyre, D.E.; Miller, R.R.; Stearns, R.A.; Tota, L.; Wyvratt, M.J.; Fischer, H.; Weber, A.E. in: Ahmed, F.; Breinlinger, E.C.; Follows, B.C.; Geiss W.B.; (Eds.), Potent, Selective and Orally Bioavailable 3-Pyridylethanolamineβ3 Adrenergic Receptor Agonists Possessing a Thiazole Benzenesulfonamide Pharmacophore, vol. 4, no, 48, Albany Molecular Research, Inc. Technical Reports, 220th American Chemical Society National Meeting, Washington, D.C., 20-24 August, 2000, Medicinal Chemistry Department, Albany Molecular Research, Inc, Albany, NY 12212-5098, 28 pp.
4. Mathvink, R.J.; Tolman, J.S.; Chitty, D.; Candelore, M.R.; Cascieri, M.A.; Colwell, Jr., L.F.; Deng, L.; Feeney, W.P.; Forrest, M.J.; Hom, G.J.; MacIntyre, D.E.; Miller, R.R.; Stearns, R.A.; Tota, L.; Wyvratt, M.J.; Fischer, H.; Weber, A.E. *Bioorg. Med. Chem. Lett.* **2000**, *10*, 1971.
5. Chung, J.Y.L.; Ho, G.J.; Chartrain, M.; Roberge, C.; Zhao, D.; Leazer, J.; Farr, R.; Robbins, M.; Emerson, K.; Mathre, D.J.; McNamara, J.M.; Hughes, D.L.; Grabowski, E.J.J.; Reider, P.J. *Tetrahedron Lett.* **1999**, *40*, 6739.
6. Ishikawa, W.; Fujiwhara, M.; Kojima, T.; Endo, T.; Kato, K. United States Patent no. 4289847.
7. Burns, S.P.; Khandhadia, P.S. "Nonazide gas generant compositions" United States Patent no. US5872329.
8. Bugalho, S.C.S.; Maçôas, E.M.S.; Cristiano, M.L S.; Fausto, R. *Phys. Chem. Chem. Phys.* **2001**, *3*, 3541.

9. Bugalho, S.C.S.; Serra, A.C.; Lapinski, L.; Cristiano, M.L.S.; Fausto, R. *Phys. Chem. Chem. Phys.* **2002**, *41*, 725.
10. Bats, J. W. *Acta. Crystallogr. B* **1976**, *32*, 2866.
11. McCrone, W.C.; Grabar, D.; Lieber, E. *Anal. Chem.* **1957**, *23*, 543.
12. Putten, N.V.; Heijdenrijk, D.; Schenk, H. *Cryst. Struct. Commun.* **1974**, *3*, 321.
13. Goddard, R.; Heinemann, O.; Krüger, C. *Acta. Cryst.* **1997**, *C53*, 590.
14. Butler, R.N.; Garvin, V.C.; Lumbroso, H.; Liègeois, C. *J. Chem. Soc. Perkin Trans. II* **1984**, 721.
15. Zhaoxu, C.; Heming, X. *J. Mol. Struct. (Theochem.)* **1998**, *453*, 65.
16. Dunkin, I.R.; Shields, C.J.; Quast, H. *Tetrahedron* **1989**, *45*, 259.
17. Chae, Y.B.; Chang, K.S.; Kim, S.S. *The Daehan Hwak Hwoejee* **1967**, *11*, 85.
18. Maier, G.; Eckwert, J.; Bothur, A.; Reisenauer, H.P.; Schmidt, C. *LeibigsAnn.* **1996**, 1041.
19. Awadallah, A.; Kowski, K.; Rademacher, P. *J. Heterocycl. Chem.* **1997**, *34*, 113.
20. Frija, L.M.T.; Khmelinskii, I.V.; Cristiano, M.L.S. *Tetrahedron Lett.* **2005**, *45*, 6757.
21. Gómez-Zavaglia, A.; Reva, I.D.; Frija, L.; Cristiano, M.L.; Fausto, R. *J. Phys. Chem. A* **2005**, *109*, 7967.
22. Gómez-Zavaglia, A.; Reva, I.D.; Frija, L.; Cristiano, M.L.; Fausto, R. *J. Mol. Struct.*, **2006**, *786*, 182.
23. Bugalho, S.C.S.; Lapinski, L.; Cristiano, M.L.S.; Frija, L.M.T.; Fausto, R. *Vib. Spectrosc.* **2002**, *30*, 213.
24. Lopes, S.; Gómez-Zavaglia, A.; Lapinski, L.; Chattopadhayay, N.; Fausto, R. *J. Phys. Chem. A* **2004**, *108*, 8256.
25. Lopes, S.; Gómez-Zavaglia, A.; Lapinski, L.; Fausto, R. *J. Phys. Chem. A* **2005**, *109*, 5560.
26. Honda, K.; Furukawa, K. *J. Mol. Struct.* **2005**, *11*, 735.
27. Chapman, O.L.; Le Roux, J.-P. *J. Am. Chem. Soc.* **1978**, *100*, 282.
28. Dunkin, I. *Spectrochim. Acta* **1986**, *42*, 649.
29. Hayes, J.C.; Sheridan, R.S. *J. Am. Chem. Soc.* **1990**, *112*, 5879.
30. Teles, J.H.; Maier, G.; Hess, B.; Schaad, L.; Winnewisser, M.; Winnewisser, B. *Chem. Ber.* **1989**, *122*, 753.
31. Himmel, H.; Junker, M.; Schnöckel, H. *J. Chem. Phys.* **2002**, *117*, 3321.
32. Pritchina, E.A.; Gritsan, N.P.; Maltsev, A.; Bally, T.; Autrey, T.; Liu, Y.; Wang, Y; Toscano, J.P. *Phys. Chem. Chem. Phys.* **2003**, *5*, 1010.
33. Otsuka, S.; Nakamura, A.; Yoshida, T. *J. Organometallic Chem.* **1967**, *7*, 339.
34. Huisgen, R.; Vossius, D.; Appl, M. *Chem. Ber.* **1958**, *91*, 1; Huisgen, R.; Vossius, D.; Appl, M. *Chem. Ber.* **1958**, *91*, 12.
35. Bondybey, V.E.; English, J.H.; Mathews, C.W.; Contolini, R.J. *J. Mol. Spectrosc.* **1982**, *92*, 431.
36. Jacox, M.E.; Milligan, D.E. *J. Chem. Phys.* **1964**, *40*, 2457.
37. Raunier, S.; Chiavassa, T.; Allouche, A.; Marinelli, F.; Aycard, J.-P. *J. Chem. Phys.* **2003**, *288*, 197.
38. Pimentel, G.C.; Charles, S.; Rosengren, K. *J. Chem. Phys.* **1966**, *44*, 3029.
39. Milligan, D.; Jacox, M. *J. Chem. Phys.* **1964**, *41*, 2838.
40. Moore, C.; Rosengren, K. *J. Chem. Phys.* **1966**, *44*, 4108.
41. Zhizhong, W. *J. Mol. Struct. (Theochem.)* **1998**, *434*, 1.
42. Durig, J.R.; Sullivan, J.; Durig, D.; Cradock, S. *Can. J. Chem.* **1985**, *63*, 2000.
43. Lett, R.G.; Flygare, W.H. *J. Chem. Phys.* **1967**, *47*, 4730.

44. Curl Jr., R.F.; Rao, V.M.; Sastry, K.V.L.N.; Hodgeson, J.A. *J. Chem. Phys.* **1963**, *39*, 3335.
45. Koput, J. *Chem. Phys. Lett.* **1995**, *242*, 514.
46. Fausto, R.; Reva, I.D.; Lapinski, L. Abstracts of the *XX IUPAC Symposium on Photochemistry*, Granada, 2004, pp. 280.
47. Chang, R. *Chemistry*, eighth ed., McGraw Hill, New York, 2005 (chapter 9.10).
48. Gómez-Zavaglia, A.; Reva, I.D.; Frija, L.; Cristiano, M.L.; Fausto, R. *J. Photochem. Photobiol. A-Chem.* **2006**, *179*, 243.
49. Reva, I.D.; Stepanian, S.G.; Adamowicz, L.; Fausto, R. *Chem. Phys. Lett.* **2003**, *374*, 631.
50. Quast, H.; Nahr, U. *Chem. Ber.-Recl.* **1985**, *118*, 526.
51. Jensen, K.A.; Due, M.; Holm, A. *Acta Chem. Scand.* **1965**, *19*, 438.
52. Reva, I.D.; Stepanian, S.G.; Adamowicz, L.; Fausto, R. *J. Phys. Chem. A* **2001**, *105*, 4773.
53. Becke, A.D. *Phys. Rev. A* **1988**, *38*, 3098.
54. Lee, C.T.; Yang, W.T.; Parr, R.G. *Phys. Rev. B* **1988**, *37*, 785.
55. Csaszar, P.; Pulay, P. *J. Mol. Struct.* **1984**, *114*, 31.
56. Schachtschneider, J.H. "Technical Report, Shell Development Co. Emeryville, CA,", 1969.
57. Frisch, M.J.; Trucks, G.W.; Schlegel, H.B.; Scuseria, G.E.; Robb, M.A.; Cheeseman, J.R.; Montgomery, J.A.; Vreven, T.; Kudin, K.N.; Burant, J.C.; Millam, J.M.; Iyengar, S.S.; Tomasi, J.; Barone, V.; Mennucci, B.; Cossi, M.; Scalmani, G.; Rega, N.; Petersson, G.A.; Nakatsuji, H.; Hada, M.; Ehara, M.; Toyota, K.; Fukuda, R.; Hasegawa, J.; Ishida, M.; Nakajima, T.; Honda, Y.; Kitao, O.; Nakai, H.; Klene, M.; Li, X.; Knox, J.E.; Hratchian, H.P.; Cross, J.B.; Bakken, V.; Adamo, C.; Jaramillo, J.; Gomperts, R.; Stratmann, R.E.; Yazyev, O.; Austin, A.J.; Cammi, R.; Pomelli, C.; Ochterski, J.W.; Ayala, P.Y.; Morokuma, K.; Voth, G.A.; Salvador, P.; Dannenberg, J.J.; Zakrzewski, V.G.; Dapprich, S.; Daniels, A.D.; Strain, M.C.; Farkas, O.; Malick, D.K.; Rabuck, A.D.; Raghavachari, K.; Foresman, J.B.; Ortiz, J.V.; Cui, Q.; Baboul, A.G.; Clifford, S.; Cioslowski, J.; Stefanov, B.B.; Liu, G.; Liashenko, A.; Piskorz, P.; Komaromi, I.; Martin, R.L.; Fox, D.J.; Keith, T.; Al-Laham, M.A.; Peng, C.Y.; Nanayakkara, A.; Challacombe, M.; Gill, P.M.W.; Johnson, B.; Chen, W.; Wong, M.W.; Gonzalez, C.; Pople, J. A. Gaussian 03, Revision C.02 ed.; Gaussian, Inc.: Wallingford CT, 2004.